Stony Brook University

Spherical Indentation to Probe Atelectasis in the Mammalian Lung

A Thesis Presented

by

Maricris Resurreccion Silva

to

The Graduate School

in Partial Fulfillment of the

Requirements

for the Degree of

Master of Science

in

Materials Science and Engineering

Stony Brook University

December 2007

Stony Brook University

The Graduate School

Maricris Resurreccion Silva

We, the thesis committee for the above candidate for the

Master of Science degree, hereby recommend

acceptance of this thesis.

Andrew Gouldstone, PhD – Thesis Advisor
Assistant Professor
Materials Science and Engineering Department

Lysa Russo, MS
Director of Industrial and Educational Outreach
Center for Thermal Spray Technology

Yingtian Pan, PhD
Associate Professor
Biomedical Engineering Department

This thesis is accepted by the Graduate School

Lawrence Martin
Dean of the Graduate School

Abstract of the Thesis

Spherical Indentation to Probe Atelectasis in the Mammalian Lung

by

Maricris Resurreccion Silva

Master of Science

in

Materials Science and Engineering

Stony Brook University

2007

The study of lung mechanics has many advantages, not only in the healthy, physiological state of the lungs, but more importantly during pathological conditions such as acute respiratory distress syndrome, chronic obstructive pulmonary disease, asthma, and ventilator induced lung injury where the mechanical properties are severely affected. In this thesis, the investigation of mammalian lung mechanics by observation of the plastic deformation behavior of the lungs under spherical indentation is presented in which atelectasis, or the closing of alveoli, is treated as a mode of quasi-plastic deformation. Load- and displacement-controlled indentations were used to determine the effects of different physiological pressures and different types of inhalation gases on the deformation behavior of the lungs. The three gases used were air, isoflurane (an anesthetic) mixed with oxygen, and a high concentration of oxygen, all of which represent gases typically used in the clinical setting. In comparing the effects of different inflation pressures, the lungs were less dentable and stiffer at the higher pressures. In comparing the effects of different

inflation gases, the dentability of lungs was highest for oxygen-inflated lungs, followed by air-inflated lungs, which is then followed by isoflurane-inflated lungs. It was also found that the lungs inflated with these three gases shared the same low strain stiffness, but different yield strains. Use of time-domain optical coherence tomography (OCT) was tested for sub-surface imaging of the lungs before and after indentation, and OCT proved a useful method for distinguishing between regions of tissue and non-tissue inside the lungs. OCT also proved a useful method for observing plastic deformation by providing cross-sectional images after indentation that show regions of collapsed and uncollapsed air spaces. The criterion for atelectasis was established to be a pressure criterion by obtaining a good agreement between OCT images and finite element (FE) models of the lung. In total, spherical indentation and optical coherence tomography proved successful in studying non-uniform plastic deformation of the lungs that are relevant to both healthy and pathological conditions.

TABLE OF CONTENTS

Chapter	Title	Page
	List of Figures ……..……..…….	vi
I	Introduction ……	1
II	The Lungs ……	5
III	Statement of the Problem ……..	10
IV	Literature Survey on Lung Mechanics …….....	12
V	Spherical Indentation …….....	15
VI	Optical Coherence Tomography ……..	17
VII	Materials and Experimental Methods …….	20
	Lung preparation	20
	Load-controlled Indentation …….....	20
	Displacement-controlled Indentation …….....	22
	Sub-surface Imaging of Plastic Deformation …….....	24
VIII	Results …….....	26
	Load-controlled Indentation ……	26
	Displacement-controlled Indentation …….	29
	Recovery of Quasi-plastic Deformation …….	33
	Sub-surface Imaging of Plastic Deformation …….	36
IX	Discussion …….....	40
X	Conclusion and Future Work …….....	46
	References	48

LIST OF FIGURES

Figure	*Title*	*Page*
1	Scanning electron micrograph of a section of a rat lung parenchyma showing alveoli, alveolar septa and an alveolar duct.	6
2	Schematic of the cellular components of lung tissue.	7
3	Pressure-volume curves for air- and saline-filled cat lungs.	12
4	Schematic of OCT scanner showing the pathway from the broadband light source (BBS), to the sample and reference arms, back to the beam splitter that directs the light to a detector after which signal processing begins to view the image in the computer.	17
5	Image of Correx 30g force gage with detachable tip for load-controlled indentation. This same force gage is used for displacement-controlled indentation.	21
6	Schematic (left) and image (right) of indenter tip used for displacement-controlled indentation.	23
7	Schematic of the time-domain optical coherence tomography system.	24
8	Schematic of indentation with a cylindrical tip.	25
9	Rabbit lungs indented with 2 g load at 6 cmH2O while inflated with (a) 100% oxygen and (b) 0.2% isoflurane.	27
10	Dog lungs indented with 3 g load at 12 cmH2O while inflated with (a) 0.2% isoflurane and (b) 100% oxygen.	27
11	Dog lungs indented with 5 g loads at 6 cmH2O while inflated with (a) 100% oxygen and (b) air.	28
12	Dog lungs indented with 5 g loads at 4 cmH2O while inflated with 0.2% isoflurane (a) immediately after lung excision and (b) 10 minutes after initial inflation.	29

13	Load vs. a/R graph of air inflated dog lungs with images displaying residual imprints from the indentation. This image depicts the deformation of the lungs as a result of two different inflation pressures, 10 cmH2O and 4 cmH2O.	30
14	Load vs. a/R graph from dog lungs inflated with 100% oxygen and 0.2% isoflurane.	31
15	Load vs. a/R graph from dog lungs inflated with air and 100% oxygen while inflated at 10 cmH2O.	32
16	Load vs. a/R graph from dog lungs inflated with air and 100% oxygen while inflated at 4 cmH2O.	32
17	Stepwise re-inflation of indented rat lungs inflated with (I) 0.2% isoflurane and (II) 100% oxygen from (a) 4 cmH2O, (b) 12 cmH2O, (c) 22 cmH2O, (d) 30cmH2O, and (e) 38 cmH2O.	33
18	Stepwise re-inflation of indented dog lungs inflated with (I) 100% oxygen and (II) air from (a) 6 cmH2O, (b) 8 cmH2O, (c) 10cmH2O, (d) 14 cmH2O, (e) 16 cmH2O, and (f) 18 cmH2O.	34
19	Dog lungs indented with 5 g loads at (a) 4 cmH2O, (b) 6 cmH2O, (c) 8 cmH2O, (d) 10 cmH2O, (e) 12 cmH2O, (f) 17 cmH2O, and (g) 20 cmH2O while inflated with (I) air, (II) 0.2% isoflurane, and (III) 2% isoflurane	35
20	OCT images of (a) collapsed and (b) inflated rat lung.	36
21	OCT images of a spherically-indented rat lung inflated with air. Image (a) is an imprint left with a 3g load at 10 cmH2O and (b) is the imprint re-inflated to 18 cmH2O.	37
22	OCT image of a spherically-indented rat lung inflated with blood gas.	38
23	OCT images of a cylindrically-indented rat lung inflated with air. Image (a) is an imprint left at approximately 6 cmH2O and (b) is the imprint re-inflated to 14 cmH2O.	39
24	OCT image of a cylindrically-indented rat lung inflated with blood gas.	39
25	Pressure distribution for axisymmetric indentation of an elastic half-space bound by a pre-tensed elastic membrane.	45
26	Pressure distribution for “rib” indentation of an elastic half-space bound by a pre-tensed elastic membrane.	45

ACKNOWLEDGMENTS

This study is financially supported by the NSF Faculty Early Career Award (CMS 0449268).

I want to take this opportunity to thank, first, my advisor, Prof. Andrew Gouldstone, for giving me this chance to expand my horizons both in academia and in research. Thank you for everything that you are teaching me, for believing in me, for the continued support, and for making this journey fun.

My special thanks go to my friend Melissa Hoyos who was with me from the beginning of this project. Thank you to Jean Rooney, Dr. Alex Romanov, and Dr. Tom Zimmerman from the Division of Laboratory Animal Resources (DLAR) here at Stony Brook for all their help in setting up the experiments and allowing us to use the facilities in DLAR. Thank you to Dr. Joan Zuckerman, Dr. Irvin Krukenkamp and Alyssa Tuthill for providing us with the lung tissues used in our experiments. To Dr. Yingtian Pan and his graduate students, Zhijia Yuan and Zhenguo Wang for allowing and helping us to use their OCT system. To Meng Qu and Jae Hun Kim, thank you for helping me with the experiments, and to Jae for the finite element models included in this thesis.

My sincere appreciation also goes to my committee members, Lysa Russo and Dr. Yingtian Pan for their support in writing this thesis.

To all my friends in the Center for Thermal Spray and my best friends,, Christine, Laura and Mina, thank you for having been there for me.

To my family, thank you for always being there and supporting my every decision. You are my inspiration and this thesis is for you. Lastly, I want to thank my husband for his love, patience, and support. I am grateful to you for always encouraging me, believing in me, and for always making me laugh, especially when sometimes I don't think I have time for it. Thank you so much for waiting.

I. INTRODUCTION

A reported number of people suffer from pulmonary pathological conditions such as acute respiratory distress syndrome (ARDS), chronic obstructive pulmonary disease (COPD), and asthma that affect their normal lung mechanics. Unfortunately, ventilation treatment for the mentioned pathologies may cause ventilation induced lung injury (VILI) that results in further insult to the lungs. During normal breathing, the lungs, most importantly the alveolar structures must efficiently expand and contract to allow the proper exchange of gasses essential for living. The lungs undergo uniform deformation where they require compliance ($\Delta V/\Delta P$) during inflation or inhalation, and recoil during deflation or exhalation. The lungs also undergo non-uniform deformation as they slide and press against surrounding tissues and organs like the heart and ribs where they then require structural stability typically provided most by the connective tissues that make up the alveolar walls and the surface tension-reducing surfactant that lines the alveoli. The surfactant provides stability by reducing the work required during breathing and prevents atelectasis, which is the localized collapse of alveoli. Normal lung mechanics should be, and usually is, very efficient during breathing. However, in pathological conditions, the normal lung mechanics are severely affected.

To date, the prevalence of ARDS is a reported 12.6 to 18 per 100,000 people per year, but due to differing criteria for characterization, the numbers are believed to be much higher[4, 5]. In ARDS, the symptoms include acute lung injury that causes increased permeability and inflammation of the lung parenchyma,

acute hypoxia, and increased dead space. A decrease in lung compliance is also reported due to both increased deposition of collagen and changes in the chemical structure of surfactant[6]. The symptoms manifest within 24-72 hours of the time of lung insult. However, the specific triggers such as physical (e.g. trauma) or chemical (e.g. smoke) injury to the lungs are not known. The lungs undergo three stages in the progression of ARDS and these include the exudative phase, proliferative phase and fibrotic phase. In the proliferative phase, the tendency for alveolar collapse is increased due to the damage of the cellular components of the lung parenchyma, which includes injury and proliferation of type II cells that are responsible for producing the surfactant[4]. Due to this effect in the surfactant, administration of exogenous surfactant has been tested and although mortality rates decreased in neonates, no improvements were seen in adult patients[5]. Therefore, as the disorder progresses into the irreversible fibrotic phase, both pharmacologic and ventilatory support care becomes necessary to improve oxygenation that is no longer being provided by the lungs.

COPD, like ARDS, also requires pharmacologic and ventilatory support care to improve ventilation. According to Barnes, COPD is the result of "long-term exposure to inhaled noxious gases and particles" including cigarette smoke which accounts for the majority of cases of COPD in developed countries[7]. It is a growing health problem and is now ranked fourth as the most common cause of death in the world. COPD includes both chronic bronchitis and emphysema and is usually characterized by airway blockage due to inflammation and increased mucus secretion, and small airway collapse due to decreased lung elasticity and severed alveolar attachments that serve to support these small airways. In COPD, the functional residual capacity is increased as well as the work required for breathing. Because of the narrowing of the airways, reduction in recoil, as evidenced by hyperinflation of the lungs at rest, is a common abnormality

associated with COPD that becomes even more pronounced during exercise or heavy breathing[7, 8]. Extreme care must then be taken during ventilatory support in order not to abuse the lungs even further.[9]

Lastly, asthma is yet another pathological condition that may require mechanical ventilation, especially during periods of acute asthma attacks. It is one of the most common causes for hospitalization or emergency room visits particularly among children, and it is a very life-threatening condition if not managed properly[10]. It is a chronic disease triggered by a wide range of nuisances including allergies, exercise, and gas particles in the air. It is characterized by periodic wheezing and/or coughing and difficulty breathing due to the narrowing of the airways caused by increased production of mucus and contraction of the smooth muscles that surround the airways. In asthma, expiratory flow, which requires lung recoil, is impaired. According to Hoppin, lung recoil is decreased in asthma due to "changes in surfactant, stretching of connective tissues, and growth[11]."

From the three mentioned pathologies, as well as during surgery when patients are under general anesthesia and for patients on life support, all may require mechanical ventilation with ventilator settings that have been reported to induce ventilator induced lung injury[12]. VILI is a complication clinically and pathologically impossible to differentiate from ARDS. Many studies over 30 years have been done to determine the cause of this injury and to understand how to improve ventilator settings to avoid this complication[13-16]. Although the degree of VILI is dependent upon both ventilator settings and the condition of the patients' lungs, more and more studies point to the benefit of pressure-controlled ventilation by maintaining a positive-end expiratory pressure during breathing while minimizing the change in lung volume, i.e. lowering the tidal volume.

As established from the mentioned pathologies as well as problems with the current ventilation treatment, there are great benefits to understanding lung mechanics, not only in normal healthy conditions, but more importantly during pathological conditions. In this thesis, the investigation of mammalian lung mechanics by observation of the plastic deformation behavior of the lungs under spherical indentation is presented, as well as brief introductions to the cellular and non-cellular framework of the lungs (Chapter II), spherical indentation (Chapter V), and optical coherence tomography (Chapter VI).

II. THE LUNGS

The lungs are the main organ of the respiratory system responsible for the proper exchange of gases during breathing. It is responsible for delivering oxygen into the bloodstream while taking carbon dioxide out. It is a very intricate system of branching airways and septal borders that divide the airspaces. These airways and airspaces are arranged in such a way that all are connected to the environment during breathing. The lungs are enclosed by a pleural membrane and are surrounded by a complex network of pulmonary capillaries with which gas is exchanged.

In mammalian lungs, the airways form a system that can be divided into three separate zones: the conducting zone, the transitional zone, and the respiratory zone[17]. The conducting zone includes the airways not in contact with the capillaries and includes the trachea, bronchi, bronchioles and terminal bronchioles. The only function of the conducting zone is to deliver inspired air into the gas exchange units of the lungs. The transitional zone, as the name states, serves as the transition region from the conducting zone to the respiratory zone. Here, the airways are very closely linked to the alveoli and some exchange of gases with the capillaries takes place. The transitional zone comprises the respiratory bronchioles and the alveolar ducts. Last is the respiratory zone which consists of all the alveoli and the network of capillaries that surround them. The respiratory zone is where gas exchange takes place and in which the alveoli are the main units of gas exchange.

In this study, more focus will be given to the respiratory zone, and more specifically to the alveoli. The lungs during indentation are not perfused and so considerations of blood flow or the effects of capillaries with blood flow on lung mechanics are neglected.

The alveoli can be described as a honeycomb- or froth-like structure in which the air spaces are divided by septal borders. Adjacent alveoli share septal borders, and overall, the alveoli comprise a very large surface area for gas exchange. Figure 1 below shows a scanning electron micrograph of a section of a rat lung parenchyma.

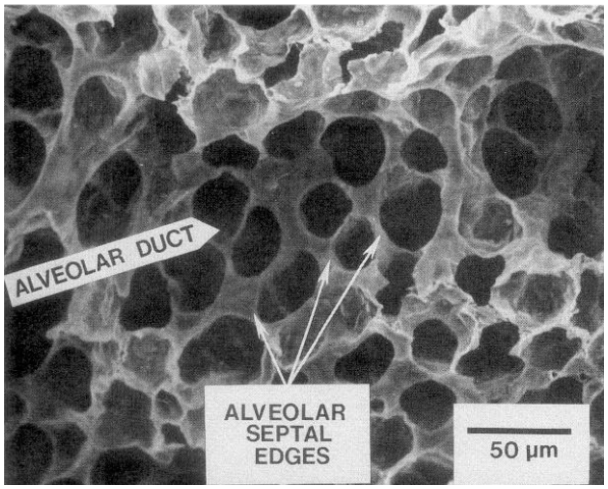

Figure 1. Scanning electron micrograph of a section of a rat lung parenchyma showing alveoli, alveolar septa and an alveolar duct. This image is taken from Mercer, R.R., M.L. Russell, and J.D. Crapo. *Alveolar septal structure in different species*. Journal of Applied Physiology, 1994. 77(3): p. 1060-1066..[3]

For mammalian lungs, the size of the alveoli and the alveolar septa depend on the species, body size and the degree of oxygen consumption[3, 17]. For humans with a body weight of 68,000 ± 3,000 g, the diameter of an alveolus can range from 210-300 μm. For rats and rabbits however, the diameter of an alveolus is much smaller and can range from approximately 90-100 μm[3, 17].

Looking closer into an alveolus, it can be seen that cells and connective tissues make up the alveolar septal borders. The septa consist of three layers which include the epithelium, the interstitium and the endothelium. The endothelium will not be discussed, but note that this layer comprises the cells and tissues that line the pulmonary capillaries. The different types of cells that make the alveolar epithelium include types I, II and III epithelial cells. Figure 2 shows a schematic of the cellular components of lung tissue including Types I, II, and III epithelial cells.

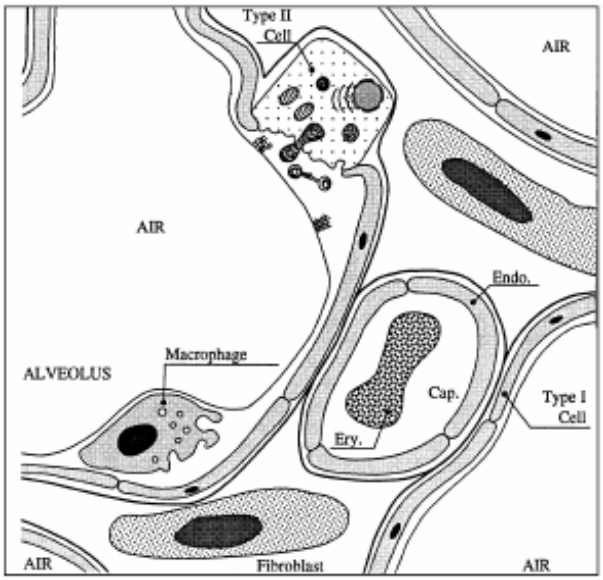

Figure 2. Schematic of the cellular components of lung tissue. This image is taken from the review paper Creuwels, L.A.J.M., L.M.G.v. Golde, and H.P. Haagsman, *The pulmonary surfactant system: biochemical and clinical aspects*. Lung, 1997. 175: p. 1-39.[2]

Type I epithelial cells are squamous cells that form the lining of the septa. They are the largest of all the cells in the septa with cytoplasmic sheets reaching a distance greater than 50 μm from the location of the nucleus, and takes up 13% of the volume distribution, 95% of the surface and 10% of the cell number in the alveolar tissue[17]. Type II epithelial cells on the other hand is about half the size of Type I cells. They take up only 9.2% of the volume distribution, but 12.3% of

the cell number in the alveolar tissue. Type II cells are secretory cuboidal cells and, although smaller than Type I cells, they have the very important task of producing the surface-lining and surface-stabilizing surfactant. Type III epithelial cells account for only 3.9% of the volume distribution and 4.7% of the cell number in alveolar tissue. They are pyramidal in shape, appear to be rare in the septa and are believed to function as receptor cells[17]. The interstitium, unlike the epithelium and endothelium, is the very thin, non-cellular layer of the septal border. This layer holds the connective tissue fibers, collagen and elastin, which are the stress-bearing components of the septa[3, 17, 18]. In the lungs, it was found that there were more collagen and elastin in the pleura than in the lung parenchyma. More specifically, there were about one-fifth more collagen and one-tenth more elastin in the pleura than in the alveolar parenchyma[19].

Beside the collagen and elastin, the other major component of the lung that contributes to its mechanical behavior is the surfactant, which, since 1929, has been known as the stabilizing agent that lines the alveoli during normal breathing[2]. During exhalation when the surface area of the lungs decreases, surface tension is decreased by the surfactant thus preventing the collapse of alveoli. After inhalation where surface area of the lungs increases tremendously, the surfactant also plays a role in recoil as higher surface tension is established in the alveoli.

The pulmonary surfactant consists of 90% lipids, of which 90% are phospholipids. Phosphatidylcholine accounts for the majority (70-80%) of the total lipid components, but cholesterol, triacylglycerol and free fatty acids can also be found. The remaining pulmonary surfactant components comprise surfactant-specific proteins that include the hydrophilic surfactant proteins (SP-A and SP-D) and the hydrophobic surfactant proteins (SP-B and SP-C). Among

these proteins, SP-A is believed to play the critical role of regulating the formation of the monolayer during breathing that reduces the surface tension.[2]

In total, the lungs comprise of several cellular components, connective tissue fibers and a surface-active liquid lining component that must all be considered when studying lung mechanics.

III. STATEMENT OF THE PROBLEM

A tremendous amount of physiological and clinical studies have been done on the bulk mechanical properties of uniform deformation of the lungs, a few have been done to study non-uniform elastic properties[20-23], but none, that we are aware of, have studied non-uniform plastic behavior of the lungs. In this study, we induce atelectasis or alveolar collapse by spherical indentation, which, at high enough compressive stress or pressure, quasi-plastically deform the lungs underneath the area of indentation.

During breathing, a healthy lung undergoes uniform deformation as it effectively expands during inhalation and contracts during expiration. A healthy lung can also experience non-uniform deformation due to gravity, chest wall interaction, vascular and bronchial pressure changes, and atelectasis[20, 23].

Atelectasis, during normal breathing, is a very common and random occurrence that can take place inside the lungs or closer to the surface of the lungs due to compression from surrounding tissues like the heart and the ribs. In this healthy state, the proper exchange of gases during breathing is not affected enough that a person will have trouble breathing or will require medical assistance. However, during pathological conditions and particularly when patients are anesthetized for surgical cases, atelectasis becomes even more pronounced as the airway passages are obstructed resulting in an increase in the local stiffness of the lungs around the atelectatic region, diminution of oxygenation, and further lung injury. In fact, atelectasis occurs in the dependent areas of the lungs for 90% of anesthetized patients[24]. With atelectatic regions, the

surrounding alveoli then have to work harder until the closed alveoli re-open. Understanding the mechanisms of atelectasis can then have a tremendous impact not only in the general appreciation of why and how it happens, but how to avoid it and properly treat it when it occurs during pathological conditions.

By treating atelectasis as a quasi-plastic deformation of the lungs (i.e. recovery of deformation does occur, not with time, but with application of high tensile pressure), indentation can be used to systematically study the mechanisms of alveolar closure. With indentation, the lung parenchyma is treated as an elastic continuum bound by and attached to a pre-tensed elastic pleural membrane with no bending resistance. By using spherical indentation with indenter tips many times greater than the size of an alveolus, the progression from elastic to plastic deformations can be observed thereby allowing insight to the mechanism of atelectasis. Spherical indenters also protect the lung tissue, especially the pleural membrane, from puncture that other sharp indenter tips can easily do with deeper indentation.

In this thesis, work on load- and displacement-controlled indentations is presented for mammalian lungs inflated at different physiological pressures with different types of inhalation gases. The three gases used are air, isoflurane (an anesthetic) mixed with oxygen, and a high concentration of oxygen, all of which represent gases typically used in the clinical setting. Use of time-domain optical coherence tomography (OCT) is tested for sub-surface imaging of the lungs before and after indentation, and the criteria for atelectasis is established by obtaining a good agreement between OCT images and finite element (FE) models of the lung.

IV. LITERATURE SURVEY ON LUNG MECHANICS

The study of lung mechanics has been a research venture for several decades now. Initially, research investigations focused on the bulk mechanical properties of lungs that centered on uniform deformation, or uniform inflation, during normal, healthy breathing that can be described by the bulk modulus. John B. West wrote a book with a chapter dedicated to the mechanics of breathing relating the contribution of both lung tissue as well as the surfactant that lines the alveoli to the bulk mechanical elastic behavior of lungs by presenting the established pressure-volume curves for air- and saline-filled lungs shown in Figure 3[1].

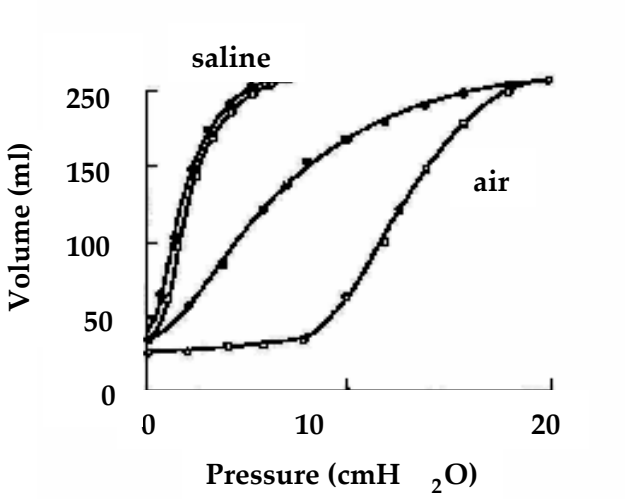

Figure 3. Pressure-volume curves for air- and saline-filled cat lungs.[1]

Here, the effects of the surfactant were minimized if not completely taken away by filling the lungs with a saline solution resulting in an increased compliance and decreased hysteresis than air-filled lungs. With these pressure-volume

curves, the bulk modulus can be easily obtained by calculating the reciprocal of the specific compliance $K = V (\Delta P/\Delta V)$[25]. Once again, this bulk modulus is used to describe lung behavior only under uniform deformation or inflation. In order to determine the behavior of the lungs under non-uniform deformation, another modulus, the shear modulus is needed and several studies have attempted to obtain this value via a similar method of indentation.

By treating the lung as an elastic continuum, Lai-Fook, Wilson, Hyatt, and Rodarte used flat punch indentation (i.e., indentation with the flat surface of a cylindrical rod) to relate load vs. displacement data to measure the modulus. In this study they found that the lungs are more deformable with shear than with dilatation and that the modulus decreased with increasing punch diameter. They suggested this may be due to the tension of the pleura which serves to support the flat punch during indentation. This finding prompted the study by Hajji who derived equations for uniform pressure indentation while taking into account the effects of a membrane on an elastic half space[21, 22]. Here he found that his analysis deviates from the classical solution, but agrees well with experimental data and so is a useful tool for obtaining the mechanical properties of the lung parenchyma as well as the pleural membrane. Hajji, Wilson, and Lai-Fook presented another study for improved measurements of shear modulus and membrane tension where they used a uniform circular load instead of a flat punch[26]. Here they found that the shear modulus of the parenchyma is a function of the transpulmonary pressure, that this modulus is independent of the species size, and that the pleural membrane contributes to approximately 20% of the work of the lung during deflation.

Other studies that used indentation include the work presented by Lai-Fook and Hyatt who tested the effects of age on the elastic moduli of human lungs. They also used flat punch indentation of the lungs and they found that the

shear modulus increases both with age and transpulmonary pressure. Coughlin Suki, and Stamenović studied the dynamic behavior of the lungs in shear using the similar approach of indentation with a rigid cylindrical flat punch. They found that the shear elastance increased with increasing frequency, decreased with increasing load, and increased with increasing lung volume.

All of these previous investigations focused on the study of uniform and non-uniform elastic deformation behavior of the lungs. Although they are very useful in pointing out the necessary considerations for deformation such as the effects of pressure, age, and the pleural membrane, none of the mentioned studies focused on non-uniform plastic deformation behavior of the lungs. Residual imprints were observed in the study by Hajji, Wilson, and Lai-Fook, but these imprints were never analyzed[26]. In this study, plastic deformation will observed using a different type of indenter geometry than the flat punch or uniform circular load. A spherical indenter will be used to study the residual imprints and to observe the effects of inflation pressure and inflation gases on plastic deformation of the lungs.

V. SPHERICAL INDENTATION

Spherical indentation is an effective method used for measuring the surface mechanical properties of materials. It has a well-known linear elastic solution established by Hertz that is valid for indentation at very small strains, i.e. for small indentation depths comparative to the radius of the spherical tip, and it can be used to obtain values of hardness and modulus as formulated by Oliver and Pharr [27]. For spherical indentation, the load-displacement relationship is given by

$$h = \left(\frac{3}{4} \frac{F}{E_{eff} R_i^{1/2}} \right)^{2/3} \qquad \textit{Equation 1}$$

where R_i is the radius of the spherical indenter and E_{eff} is the effective elastic modulus given by

$$\frac{1}{E_{eff}} = \frac{1-\upsilon^2}{E} + \frac{1-\upsilon_i^2}{E_i} \qquad \textit{Equation 2}$$

where E and ν are the Young's modulus and Poisson's ratio of the material, and E_i and ν_i are the Young's modulus and Poisson's ratio of the indenter[28]. Because of the simple geometry of a spherical indenter, this method offers several advantages that are appropriate for achieving the goals of this investigation, which is to determine the mechanism of atelectasis as it is treated as a mode of plastic deformation of the lung material.

During spherical indentation, deformation is initially fully elastic at small loads and displacements. As the indentation progresses and goes deeper into the material, fully plastic deformation begins to develop. For metals indented by a spherical indenter, yielding initiates when the mean pressure (P_m) is approximately 1.1 of the yield stress[29]. However, this may not hold true for a biological material like the lung as the pre-tensed membrane may affect the stress distribution beneath the indentation region. This transition from pure elastic to pure plastic deformation is an advantage of spherical indentation as it gets rid of the elastic singularity produced at the tip of sharp indenters, such as pyramidal, conical or cylindrical punch indenters, which induces very large stresses. This method is also non-destructive which makes it an appropriate method for this study as intact lungs are required for understanding atelectasis and the role of the pleura as a protective membrane.

VI. OPTICAL COHERENCE TOMOGRAPHY (OCT)

In this study, spherical indentation was used for observing plastic deformation at the surface of the lungs. To understand the mechanism of atelectasis, sub-surface observations of plastic deformation was necessary and optical coherence tomography was tested for this purpose. There are many technologies and/or methods used to look inside the lungs, and optical coherence tomography is a promising method for this study as it offers real-time imaging of the lungs without affecting the results of the indentation. OCT is known to offer non-invasive and non-contact cross-sectional imaging of biological tissues to a depth of a few millimeters with micrometer-scale resolution. Depending on the type of tissue, the penetration depth achieved by OCT can be up to 3 millimeters. The detailed theory and principles of OCT have already been described in previous studies and texts[30-37], so only very briefly will it be described here. Figure 4 shows a system level schematic of an OCT system.

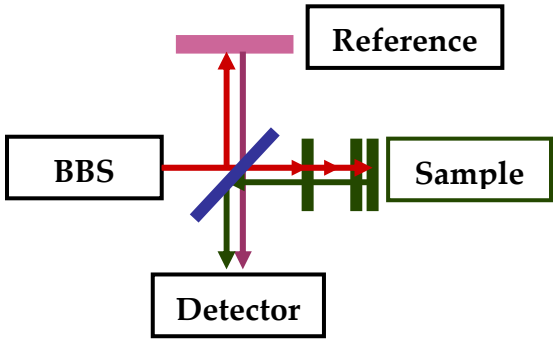

Figure 4. Schematic of OCT scanner showing the pathway from the broadband light source (BBS), to the sample and reference arms, back to the beam splitter that directs the light to a detector after which signal processing begins to view the image in the computer.

Very simply, a time domain-OCT (TD-OCT) system uses a broadband, low-coherence, near-infrared light source with a central wavelength between 700-1350 nm. The light enters a Michelson interferometer which includes a beam splitter that splits the light fifty-fifty with half of the light going to the reference arm and the other half illuminating and scanning the sample. The reference arm incorporates a mirror that moves or scans at a very high but constant speed. Light that reflects back from the sample arm and the reference arm are recombined at the beam splitter which then directs the light to a photodiode that detects the signal. Because the speed of light is so fast in the back reflection from the sample arm, a reference arm is needed to interfere with light from the sample arm, thus slowing it down enough to be detected. So, in principle, OCT depicts the intensity of back-scattered interference where, in general, if the pathlengths of the light that gets reflected back from both arms match to at least within the coherence length, then interference will occur.

Once the light is detected by the photodiode, the signal gets processed by a series of steps that include passing through a preamplifier, a bandpass filter, an envelope detector or demodulator (i.e., measures the intensity only) and an analog-to-digital converter before being able to view the image in the computer. OCT uses a point-scanning method that incorporates both depth and lateral scanning. Decoupling of this point-scan provides the two-dimensional image typically provided by OCT systems. Three-dimensional images can also be achieved with OCT with movement of the sample stage in a direction orthogonal to both the axial and lateral scanning directions.

In OCT, the axial and lateral resolutions are determined by the light source and the focusing conditions respectively[38]. A broadband source is used in

OCT because this usually means a higher axial resolution as can be deduced from Equation 3 below

$$l_c = \frac{2\ln 2}{\pi}\frac{\lambda_o^2}{\Delta\lambda} \qquad \textit{Equation 3}$$

where l_c is the axial resolution, λ_o is the central wavelength of the light source, and $\Delta\lambda$ is the source bandwidth. The lateral resolution, on the other hand, is usually controlled by the ability to the light in terms of how it is directed as well as collected.

VII. MATERIALS AND EXPERIMENTAL METHODS

None of the animals were raised nor sacrificed specifically for these experiments.

Lung preparation

Dogs and rabbits of either sex were all euthanized with a high dose of pentobarbital sodium via intravenous injection. Rats of either sex were sacrificed using one of several methods including intravenous injection of a high dose of pentobarbital sodium, exposure to 100% carbon dioxide, or cervical dislocation. Immediately after the animals were sacrificed, the lungs were extracted from the animal, connected to a pressure-controlled ventilator via a tracheostomy tube and inflated with one of three inflation gases: air, 100% oxygen, or 0.2% isoflurane.

Throughout the experiments, the lungs were sprayed or washed with 0.9% sodium chloride, i.e. saline solution, in order to keep the lungs moist at all times. The experiments were also limited to one hour to avoid drying of the lungs or changes in its mechanical properties.

Load-controlled indentation

For the load-controlled indentation experiments, a spherical bead was attached to the tip of the Correx 30g force gage shown in Figure 5 below.

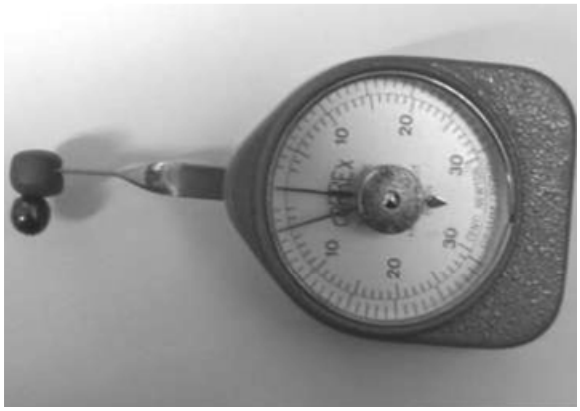

Figure 5. Image of Correx 30g force gage with detachable tip for load-controlled indentation. This same force gage is used for displacement-controlled indentation.

The lungs, already connected to the ventilator were inflated with one of the three inflation gases to 25-30 cmH_2O. The lungs were then deflated and inflated from a high pressure (20-25 cmH_2O) to a low pressure (2-5 cmH_2O). This cycle was repeated up to 10 times, first, to remove any atelectatic regions and, second, to ensure that the entire lung parenchyma was exposed to the inflation gas being introduced. After the final deflation of the cycle, the lungs were re-inflated to physiologic pressures corresponding to the lower and upper limits of the tidal volume (i.e., the pressures encountered by the lungs during normal breathing) which are 4-6 cmH_2O and 10-12cmH_2O, respectively. The lungs were held in either one of the mentioned pressures and indented with a 3-5g load. Pictures were taken of the residual imprints left by the indentation, and the recovery behaviors were observed by a step-wise re-inflation of the lungs up to pressures corresponding to deep breathing (20-25cmH2O) or until full recovery of the imprints were achieved. Pictures were also taken for every inflation pressure step.

Once the imprints fully recovered, the lungs were then re-inflated with a different inflation gas than previously used in the first set of steps and the same cycling, indentation and step-wise re-inflation were performed to observe the

effects of different inflation gases on the dentability of the lungs. Due to the time constraints, the lungs were inflated with only two inflation gases per experiment.

Displacement-controlled indentation

The displacement-controlled indentations were conducted in a similar approach to that of load-controlled indentation using a similar Correx force gage. For this set of indentation experiments, the tip was replaced with a ping pong ball modified as shown in Figure 6 below, which includes a schematic of the silver markings on the ball and an image of an indenter tip marked for a specific contact radius. For the actual indenter used, concentric circles were drawn to mark various contact radii and hence depth displacements. Strips of silver paint were painted on the ball as shown in the schematic with each strip painted up to the perimeter of a specific circle. A main silver line (M) was painted to contact all the circles up to the perimeter of the smallest marked circle. The silver strips were then connected to copper wires shown in the image, which were held in place with electrical tape. These copper wires were coupled to a circuit associated with as many piezo buzzers as the number of circles: here a total of 4 were used. As the tips were used for indentation, the tissue sprayed with saline touched the perimeter of the circles and consequently the strips of silver paint with deeper indentation. This effectively closed the circuit that caused the activation of the piezo buzzers as the indentation progressed deeper into the tissue.

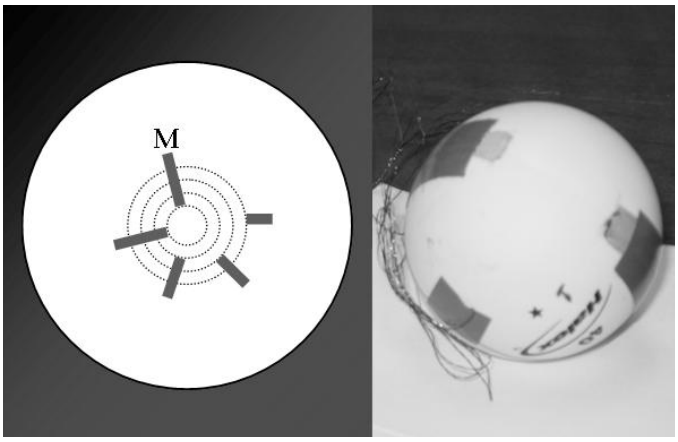

Figure 6. Schematic (left) and image (right) of indenter tip used for displacement-controlled indentation.

Unlike the load-controlled indentation, displacement-controlled indentation was used to measure the loads at specific contact radii. This method of indentation allows the measurement and comparison of the elastic and plastic deformation behavior of the lungs.

For the experiment, the lungs were inflated with one of the three mentioned inflation gases, cycled between high and low physiologic pressures as the previous experiment, held at a constant pressure and indented using the Correx force gage with the modified tip. During loading, measurements of the loads were recorded with their corresponding displacements. Pictures were taken when plastic deformation was observed on the surface of the lungs. As with the load-controlled indentation experiments, a second inflation gas was used to measure the effects of the gases on the lungs, and due to time constraints, indentation for only two inflation gases were used.

For both load- and displacement-controlled indentation, the effects of inflation pressure and inflation gas on the deformation behavior of the lungs were observed.

Sub-surface imaging of plastic deformation

In this set of experiments, only rat lungs were used. The rats were euthanized either by overdose with pentobarbital sodium or by cervical dislocation. Due to the time constraints only one inflation gas was used per experiment. The lungs of rats sacrificed with pentobarbital sodium were inflated with air. Those sacrificed by cervical dislocation were exposed to 5% isoflurane for at least 30 minutes prior to death and the lungs of these rats were inflated with blood gas (95% O_2 and 5% CO_2).

To observe sub-surface plastic deformation of the lungs, a TD-OCT system was used. The schematic of this system is shown in Figure 7 below.

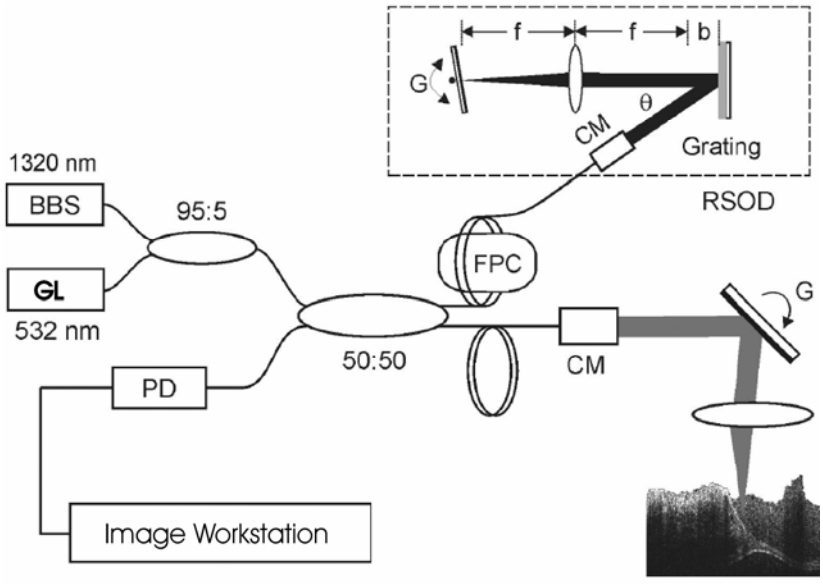

Figure 7. Schematic of the time-domain optical coherence tomography system. BBS:broadband source; CM: fiberoptic collimator; FPC: fiber polarization controller; RSOD: rapid scanning optical delay line; PD: photon diode; G: servo mirror; GL: green aiming laser.

In this system, the central wavelength used is 1320 nm with a bandwidth of 78 nm, which gives the system an axial resolution of 9.7 μm as calculated with

Equation 1. In the sample arm, the light is focused on the lung by a 4×/0.1 NA objective lens, providing a lateral resolution of 10 μm. In the reference arm, a grating-lens-based rapid scanning optical delay (RSOD) line was used to provide an axial scan of 2.8 mm in free space at a repetition rate of 1 kHz.

For the OCT experiments, the lungs were extracted immediately after the rats were killed, connected to the ventilator and inflated with air or blood gas. OCT images were taken of collapsed and inflated lungs prior to indentation. A cycling of inflation-deflation was performed to minimize atelectatic regions. Air inflated lungs were re-inflated and held at 10 cmH_2O, while blood gas inflated lungs were held at approximately 6 cmH_2O. The lungs were then indented with a spherical indenter with a 3 g load. OCT images were taken after indentation to observe the deformation. Recovery was also observed with step-wise re-inflation of the lungs. When fully recovery of the dent was achieved, the lungs were deflated to the same pressure before spherical indentation (10 cmH_2O for air-inflated lungs, 6 cmH_2O for blood gas-inflated lungs) and indented with a cylindrical indenter oriented as shown in Figure 8. A cylindrical tip was used to mimic indentation of the lungs as they press against the ribs during breathing. OCT images were taken after indentation to observe the deformation and recovery was observed with step-wise re-inflation of the lungs.

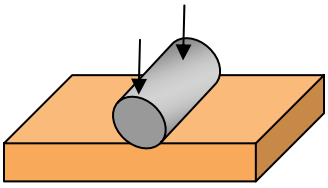

Figure 8. Schematic of indentation with a cylindrical tip.

VIII. RESULTS

Load-controlled indentation

In comparing the dentability of the lungs for load-controlled indentation, it was found that, for the same load, the lungs were more dentable when inflated at lower pressures than at higher pressures. This was also evidenced from displacement-controlled indentation shown in Figure 12, where, remember, pictures were taken only when residual imprints were observed. Here, residual impressions on lungs inflated at 10 cmH_2O with air were first observed at much higher loads (average = 36.17 g) and higher strains (average a/R = 0.583) than when the lungs were inflated at 4cmH_2O at which plastic deformation was first observed at an average load of 31.83 g and an average a/R of 0.544.

In comparing the dentability of lungs inflated with different inflation gases, marked differences were observed in the residual imprints left by the indentation. Differences in recovery behavior were also observed during re-inflation with the three different gases.

When the lungs were inflated with 100% oxygen first and 0.2% isoflurane last, it was found that with load-controlled indentation, the lungs were substantially more dentable when inflated with 100% oxygen than with 0.2% isoflurane. Figure 9 shows this result for an oxygen- and isoflurane-inflated rabbit lung indented with a 2 g load while inflated at 6 cmH_2O. Figure 10 shows the load-controlled indentation result for a dog lung indented with 3 g loads while inflated first with 0.2% isoflurane and then 100% oxygen. Here the

inflation pressure was higher at 12 cmH_2O and the same result was observed that inflation with 100% oxygen made the lungs more dentable than lungs inflated with 0.2% isoflurane. In this figure, the residual imprints are not as impressive as that in Figure 9 which repeats the observation that the dentability of the lungs decrease with higher pressures.

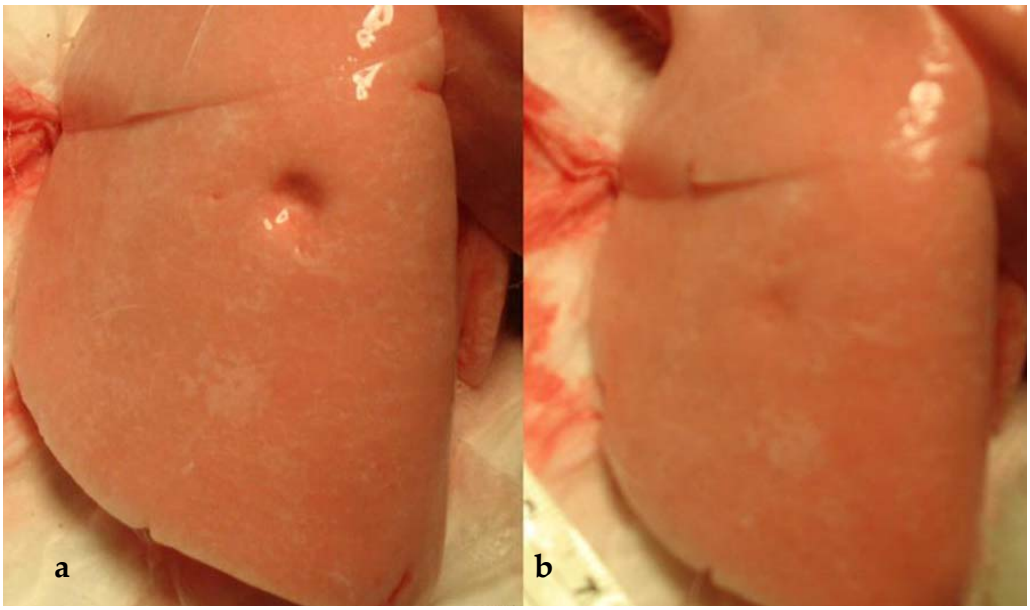

Figure 9. Rabbit lungs indented with 2 g load at 6 cmH_2O while inflated with (a) 100% oxygen and (b) 0.2% isoflurane.

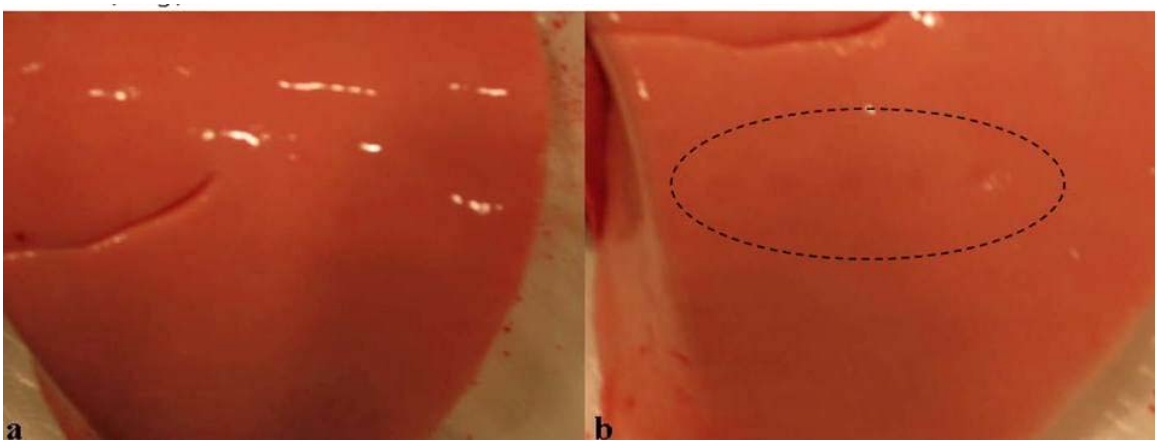

Figure 10. Dog lungs indented with 3 g load at 12 cmH_2O while inflated with (a) 0.2% isoflurane and (b) 100% oxygen.

When the lungs were inflated first with 100% oxygen and then air, the imprints seen in Figure 11 were observed. The lungs were more dentable in 100% oxygen than in air, although the difference was not as pronounced when the lungs were inflated with 100% oxygen and 0.2% isoflurane. The same result was found for lungs inflated first with air, then 100% oxygen.

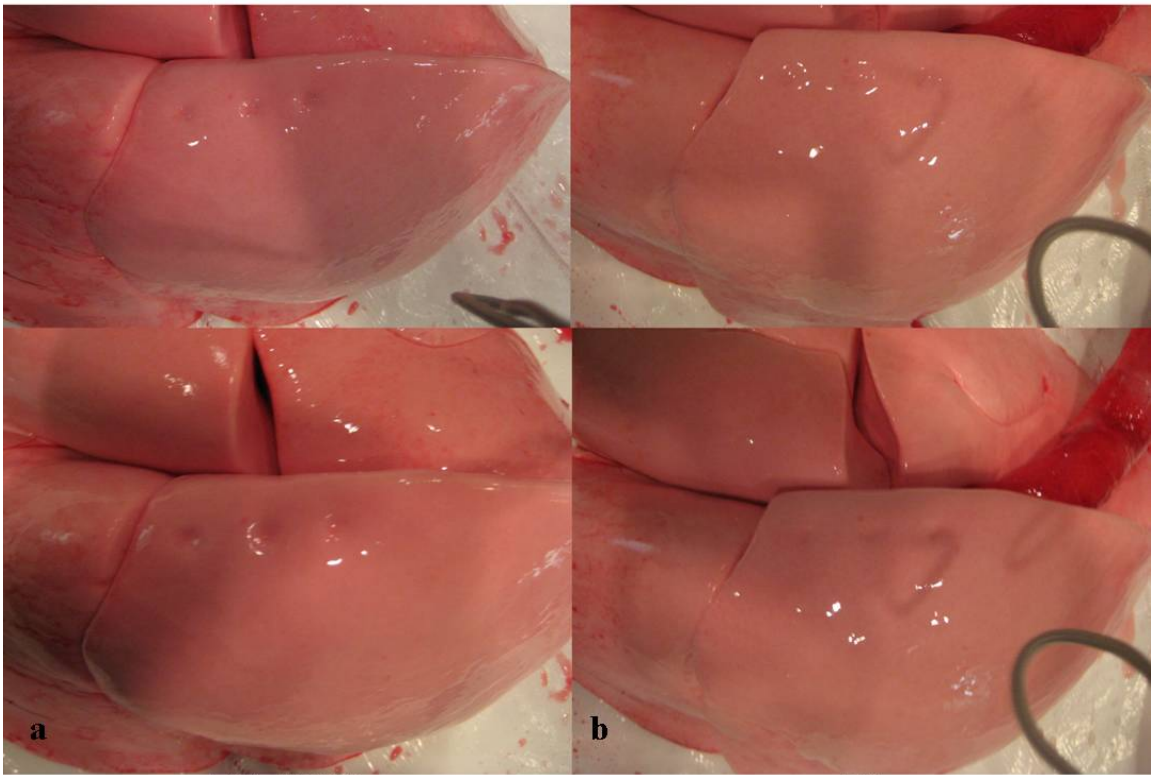

Figure 11. Dog lungs indented with 5 g loads at 6 cmH_2O while inflated with (a) 100% oxygen and (b) air.

The dentability of the lungs was also compared for lungs inflated first with air and then isoflurane. For rat lungs, the difference in dentability was not immediately obvious. Figure 19 shows the results for indented dog lungs inflated with air, 0.2% isoflurane and 2% isoflurane. Initially at 0.2% isoflurane, the isoflurane-inflated lungs appeared more dentable than with air. However, with a higher concentration of isoflurane of 2%, the pictures show that the lungs

inflated with air were more dentable than with 2% isoflurane. To test whether the effects of isoflurane becomes apparent with time, or only with concentration, indentation for lungs inflated with 0.2% isoflurane at different times was performed. Figure 12 shows the result of 0.2% isoflurane-inflated lungs and, with time, 0.2% isoflurane makes the lungs less dentable with longer time exposure.

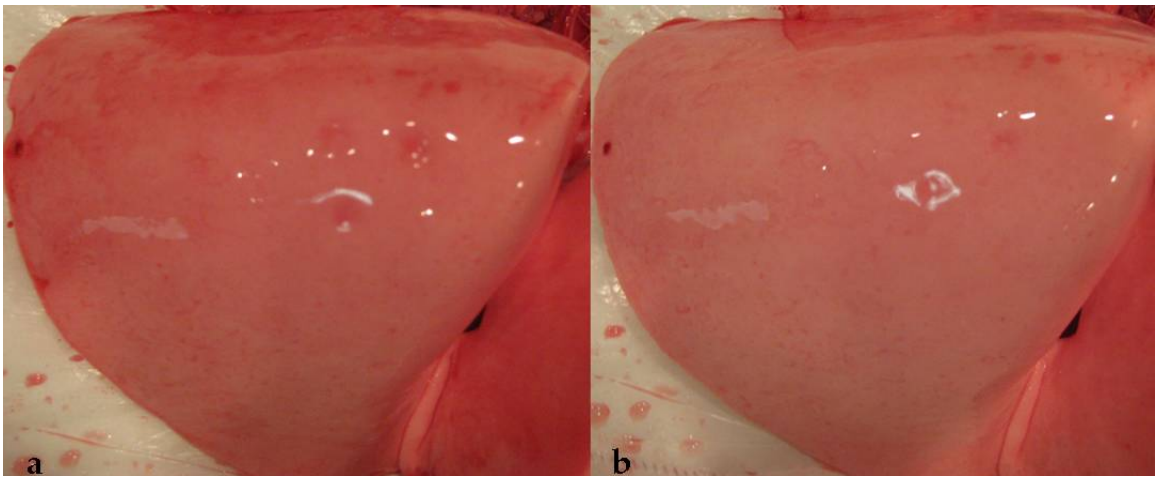

Figure 12. Dog lungs indented with 5 g loads at 4 cmH_2O while inflated with 0.2% isoflurane (a) immediately after lung excision and (b) 10 minutes after initial inflation.

Displacement-controlled indentation

For displacement-controlled indentation, deformation behavior under different inflation pressures was tested and Figure 13 shows the result for air-inflated dog lungs. It can be seen that higher loads were required to reach the same strains for lungs inflated at the higher pressure. Plasticity was also observed at lower loads and lower strains for lungs inflated at 4 cmH_2O than when the lungs were inflated at 10 cmH_2O. The same results were found for lungs inflated with 0.2% isoflurane and 100% oxygen.

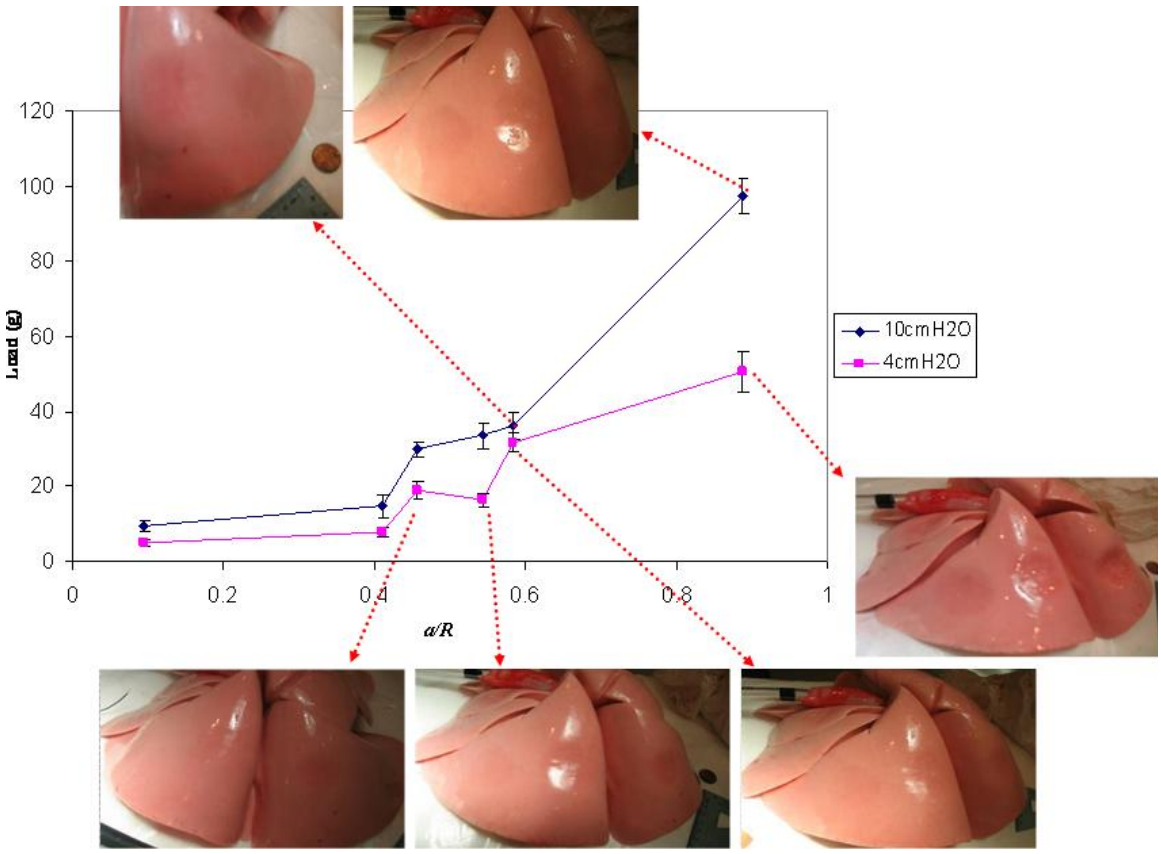

Figure 13. Load vs. a/R graph of air inflated dog lungs with images displaying residual imprints from the indentation. This image depicts the deformation of the lungs as a result of two different inflation pressures, 10 cmH_2O and 4 cmH_2O.

For inflation of the lungs with the three inflation gases, it was found that the same load is required to reach the same low strains. However, with deeper indentation, deformation behavior of oxygen-inflated lungs deviates from that of isoflurane-inflated lungs where oxygen-inflated lungs deform more at the same loads. Figure 14 shows this result with a graph of the load vs. a/R for both oxygen- and isoflurane-inflated lungs. In this figure the load vs. a/R graph was derived from the average loads from 8 different loading areas on the dog lung inflated first with 100% oxygen, and then with 0.2% isoflurane.

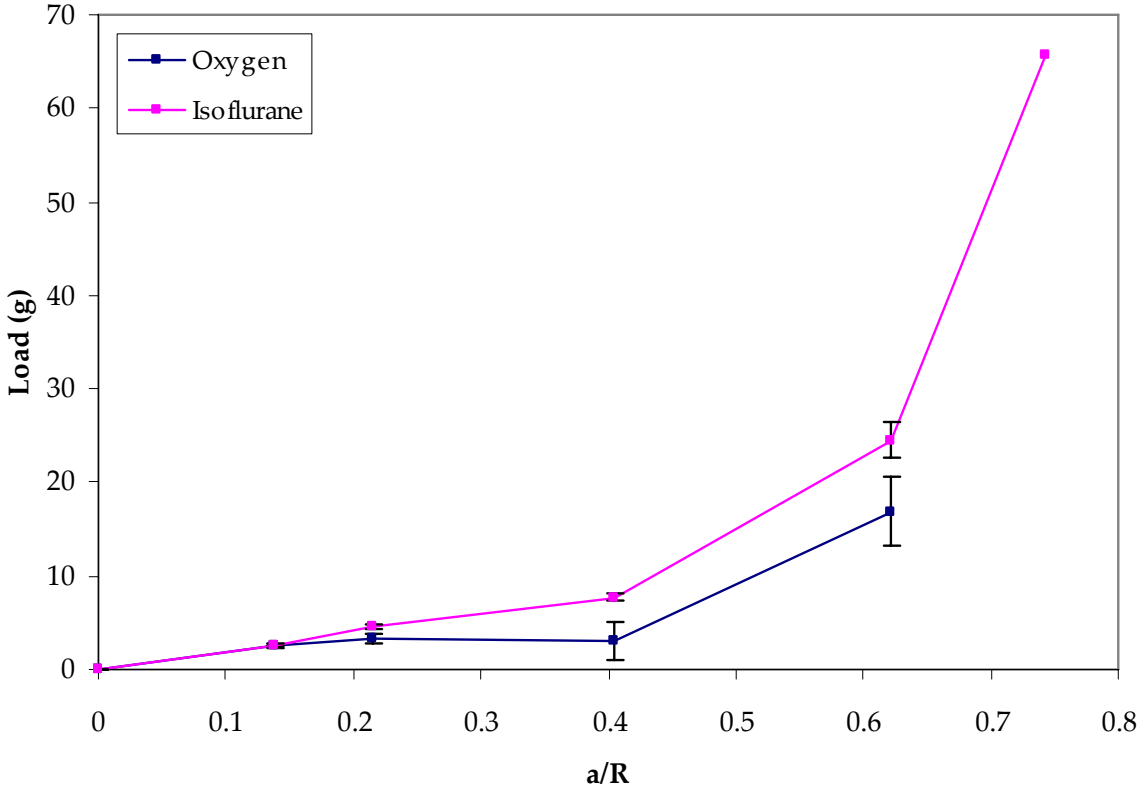

Figure 14. Load vs. a/R graph from dog lungs inflated with 100% oxygen and 0.2% isoflurane.

In Figures 15 and 16, the load vs. a/R graphs were derived from the average loads from 6 different loading regions on the dog lungs inflated first with air, then 100% oxygen. In Figure 15, the lungs were inflated at 10 cmH_2O during indentation, while the lungs in Figure 16 were inflated at 4 cmH_2O. In both cases, the same load was reached at the smallest measured displacement for both air and 100% oxygen. However, deformation behavior of oxygen- and air-inflated lungs deviated with deeper indentation where higher loads were required to reach the same strains for air-inflated lungs.

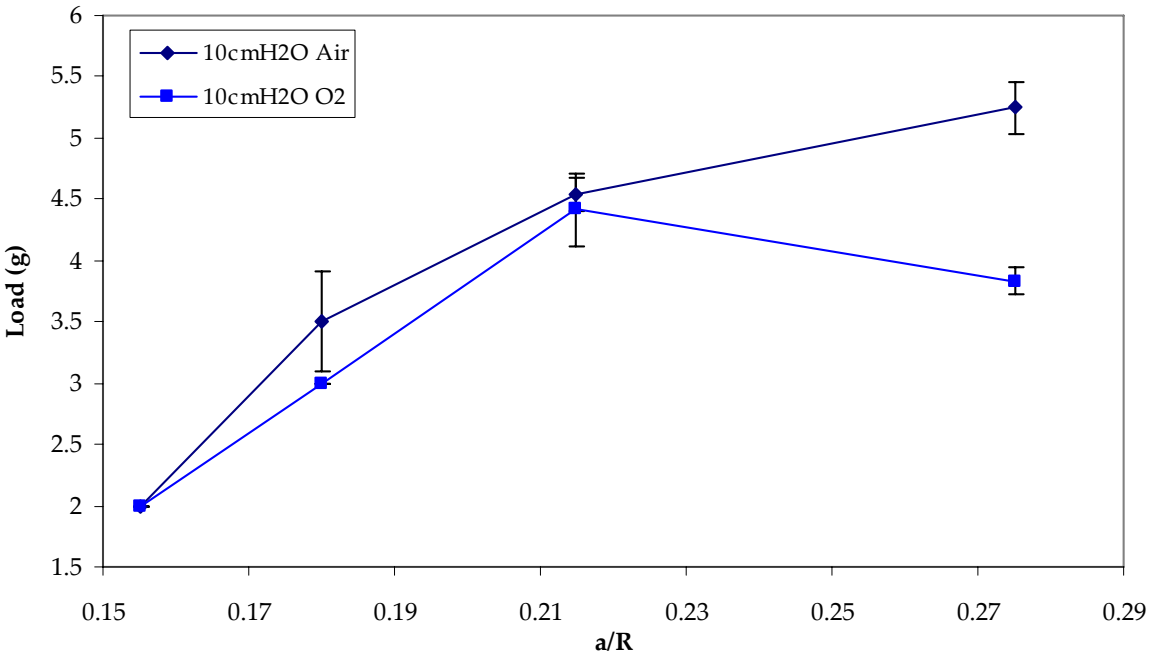

Figure 15 Load vs. a/R graph from dog lungs inflated with air and 100% oxygen while inflated at 10 cmH_2O.

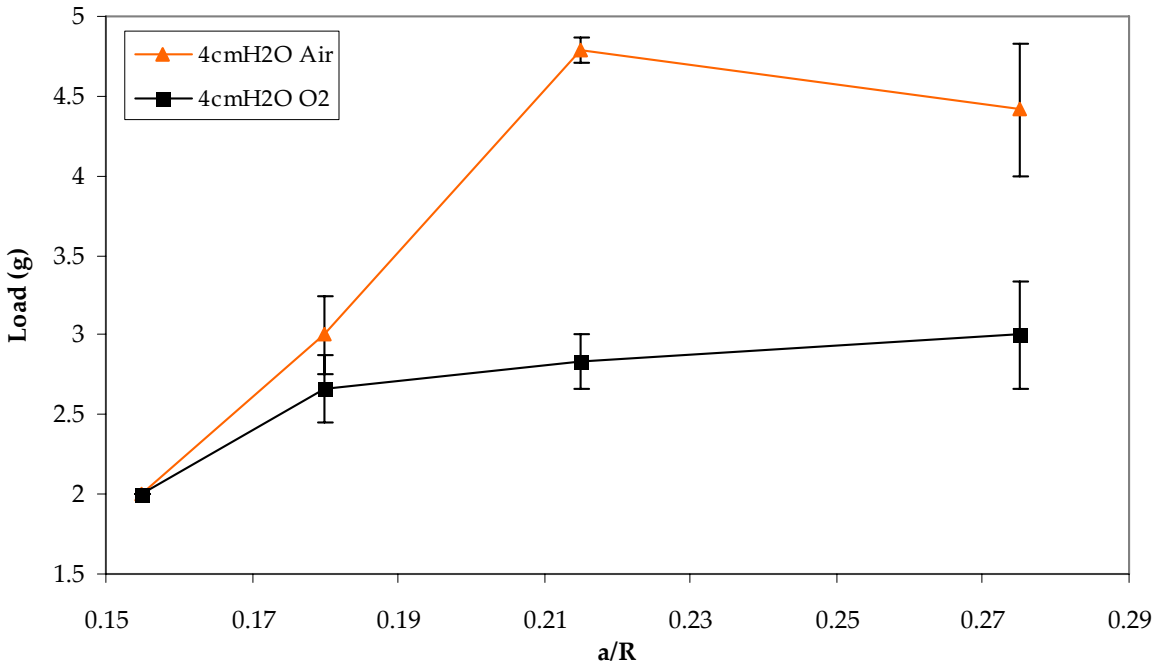

Figure 16. Load vs. a/R graph from dog lungs inflated with air and 100% oxygen while inflated at 4 cmH_2O.

Recovery of quasi-plastic deformation

After residual impressions were left on the lungs from both load- and displacement-controlled indentation, recovery behavior of the dents were observed with step-wise re-inflation of the lungs. Figure 17 shows the results of re-inflation of rat lungs with pressure steps of 4, 12, 22, 30 and 38cmH_2O. For rat lungs inflated with oxygen and 0.2% isoflurane, full recovery was achieved faster when the lungs were inflated with 0.2% isoflurane. In the figure, full recovery of the dents was observed at 38cmH_2O for isoflurane while the two dents are still clearly visible at the same pressure for oxygen-inflated lungs. When the order of inflation gases were reversed, the same results were found that recovery of the dents were achieved faster for isoflurane-inflated lungs when compared to the dents in oxygen-inflated lungs.

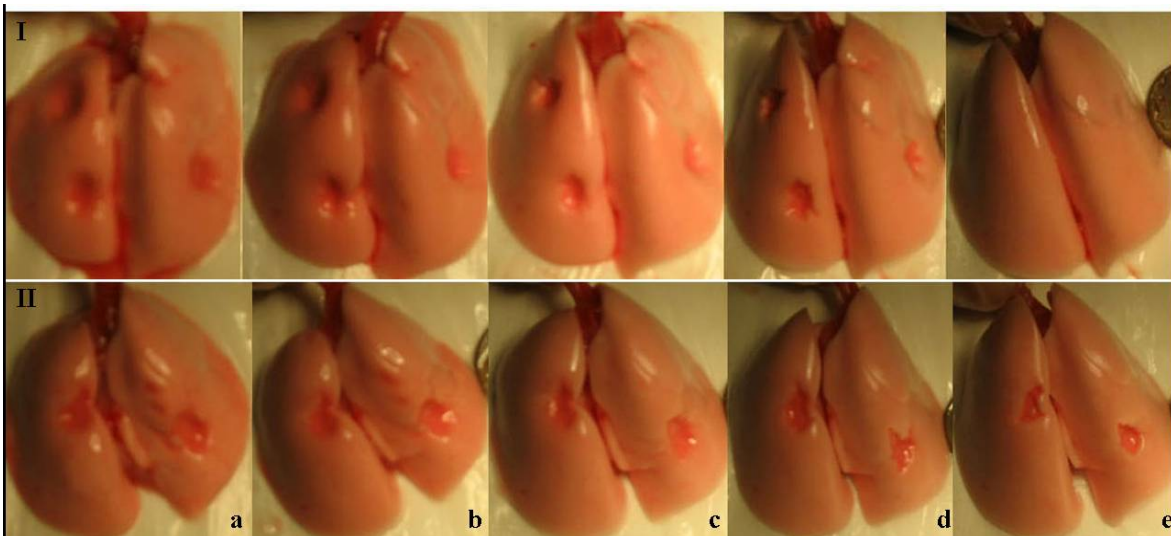

Figure 17. Stepwise re-inflation of indented rat lungs inflated with (I) 0.2% isoflurane and (II) 100% oxygen from (a) 4 cmH_2O, (b) 12 cmH_2O, (c) 22 cmH_2O, (d) 30cmH_2O, and (e) 38 cmH_2O.

In comparing the dents on lungs inflated with 100% oxygen and with air, recovery of the dents were achieved faster with air-inflated lungs. Figure 18

shows the results for a dog lung indented at 6 cmH_2O while inflated first with 100% oxygen and then with air. The inflation pressure steps included 6, 8, 10, 14, 16 and 18 cmH_2O. At the inflation pressure step of 16 cmH_2O, the three dents fully recovered for the air-inflated lung while all three dents were still visible for the oxygen-inflated lung.

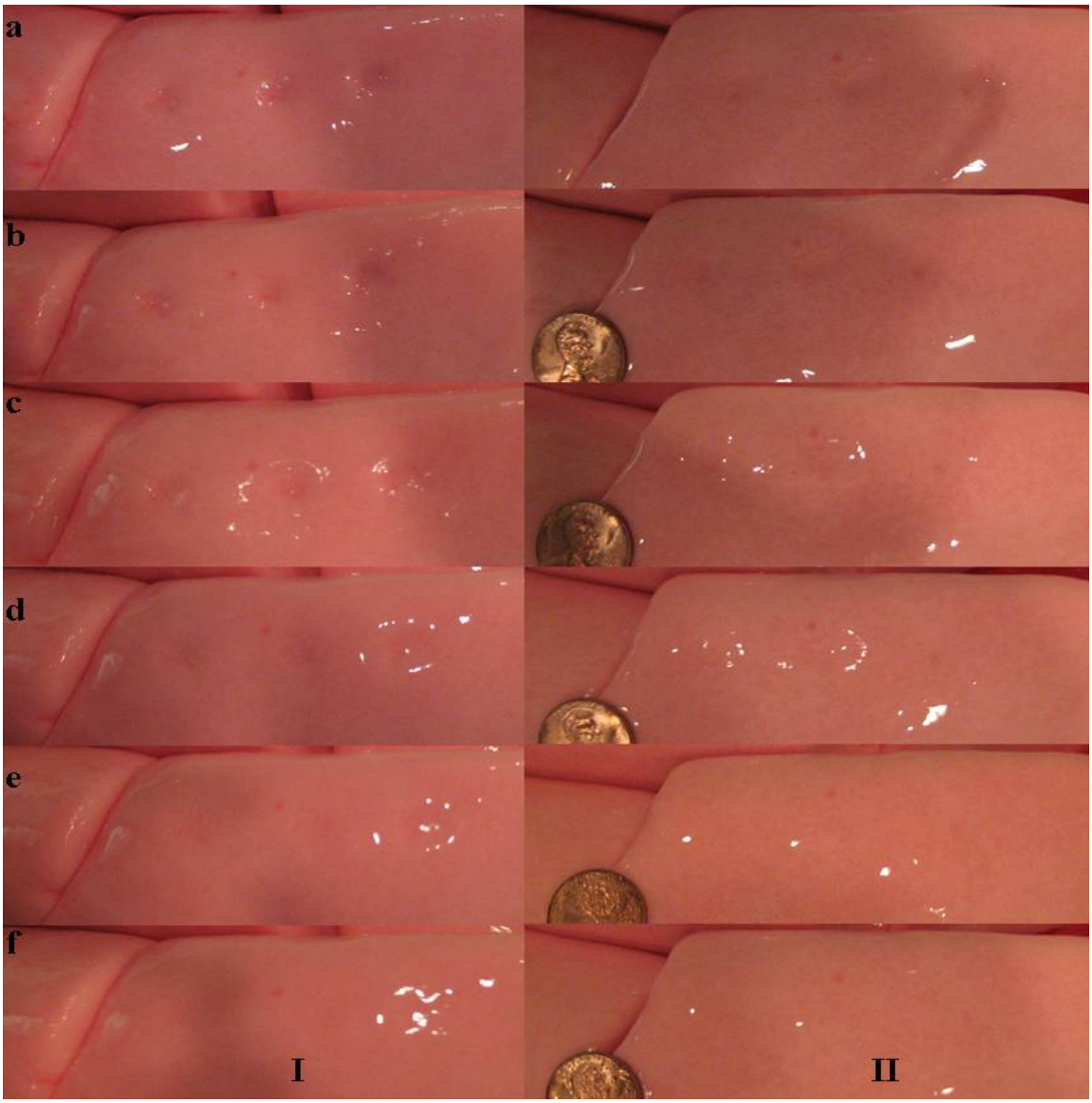

Figure 18. Stepwise re-inflation of indented dog lungs inflated with (I) 100% oxygen and (II) air from (a) 6 cmH_2O, (b) 8 cmH_2O, (c) 10cmH_2O, (d) 14 cmH_2O, (e) 16 cmH_2O, and (f) 18 cmH_2O.

Recovery behavior comparing air- and isoflurane-inflated lungs were also observed. Figure 19 show results for a dog lung inflated with air and isoflurane with inflation pressure steps of 4, 6, 8, 10, 12, 17 and 20 cmH_2O. At 20 cmH_2O, the three dents fully recovered for the lung inflated with air and 2% isoflurane. At this same pressure, the dents when the lung was inflated with 0.2% isoflurane were still slightly visible.

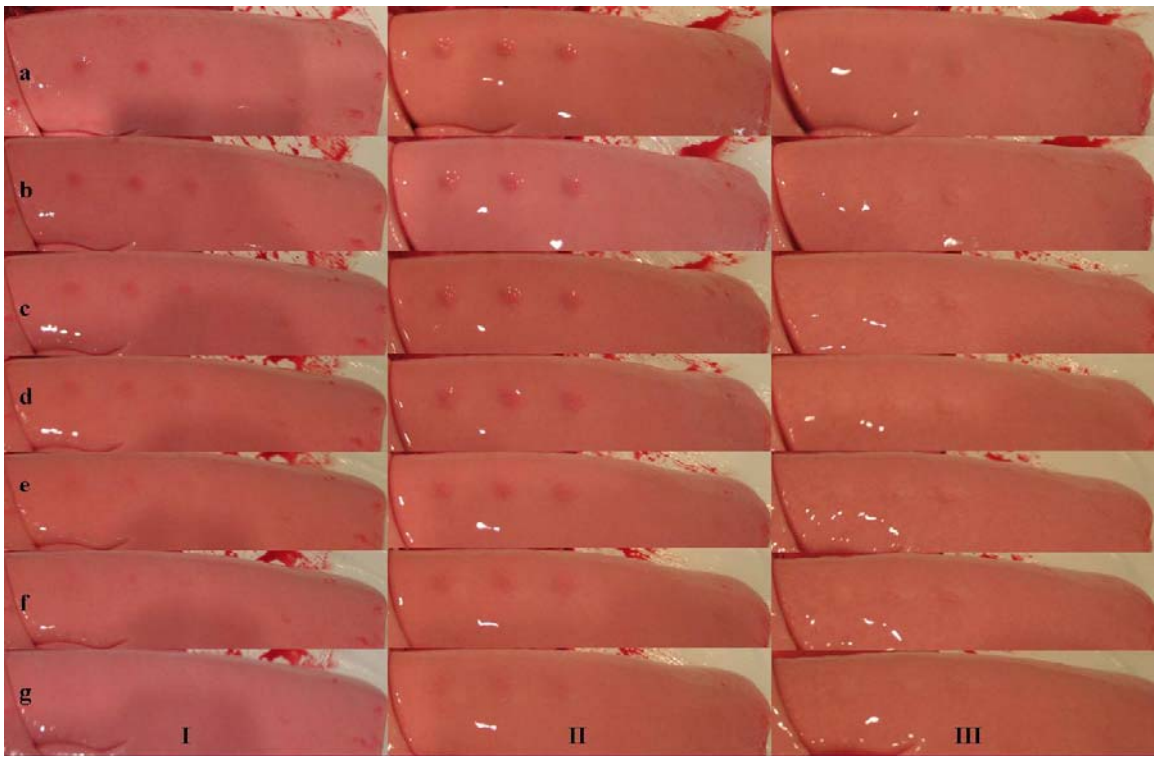

Figure 19. Dog lungs indented with 5 g loads at (a) 4 cmH_2O, (b) 6 cmH_2O, (c) 8 cmH_2O, (d) 10 cmH_2O, (e) 12 cmH_2O, (f) 17 cmH_2O, and (g) 20 cmH_2O while inflated with (I) air, (II) 0.2% isoflurane, and (III) 2% isoflurane.

Sub-surface imaging of plastic deformation

Before observing what happens underneath the region of indentation, OCT images were taken of collapsed and inflated lungs to determine whether OCT is a viable method for sub-surface imaging of the lungs. Figure 20 shows these results and it can be seen that for inflated lungs, the pleural membrane and alveoli were clearly distinguished. The surface or the membrane showed the highest intensity and the dark regions underneath the surface are the airspaces of the alveoli separated by the septal walls.

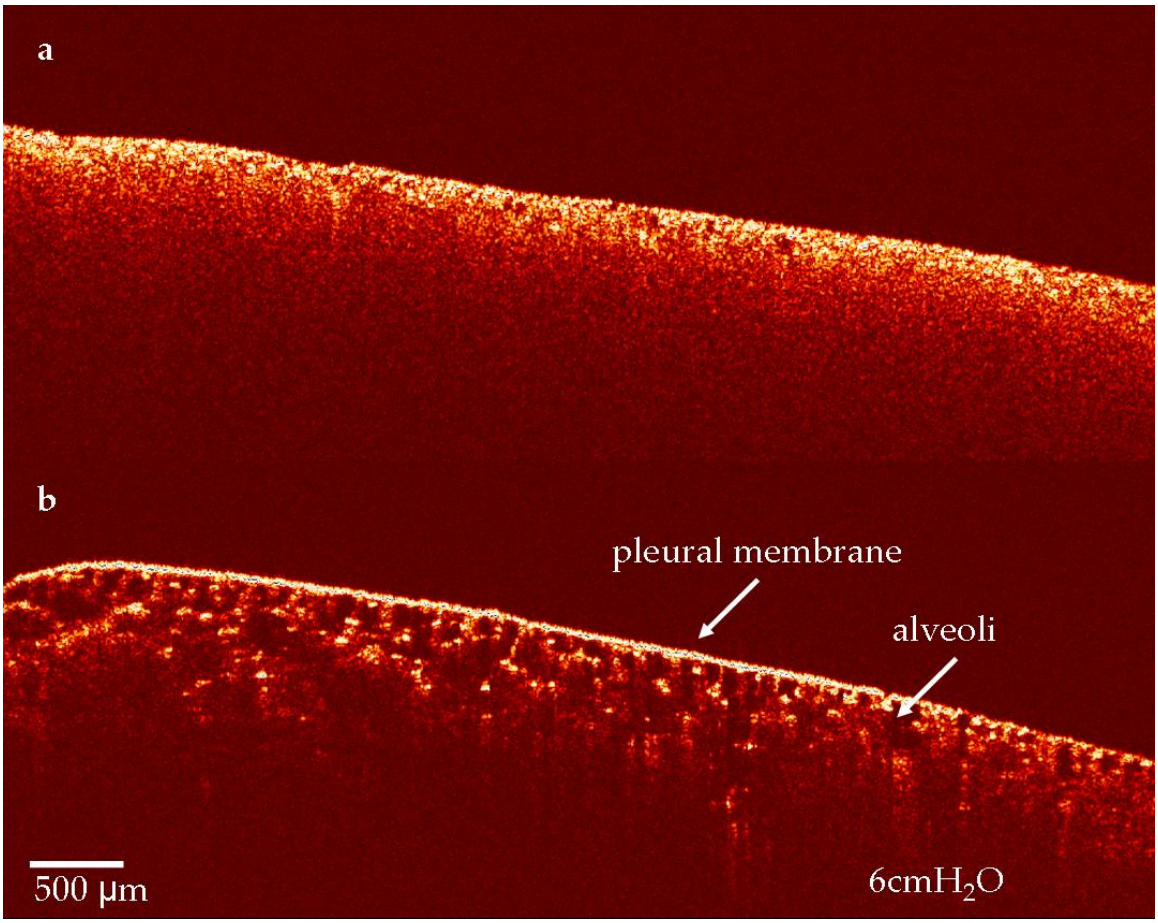

Figure 20. OCT images of (a) collapsed and (b) inflated rat lung.

Figure 21 shows OCT images of a section of the lung inflated with air and indented with a spherical indenter to 3 g. Figure 21a shows collapse underneath the indenter tip, which is evidenced by re-opening of alveoli, shown in Figure 21b, when the lungs were re-inflated to 18 cmH_2O. Notice that the opened air spaces are larger in the region of indentation in comparison to the size of alveoli in regions further from the indentation site, or even compared to the size of opened alveoli prior to indentation.

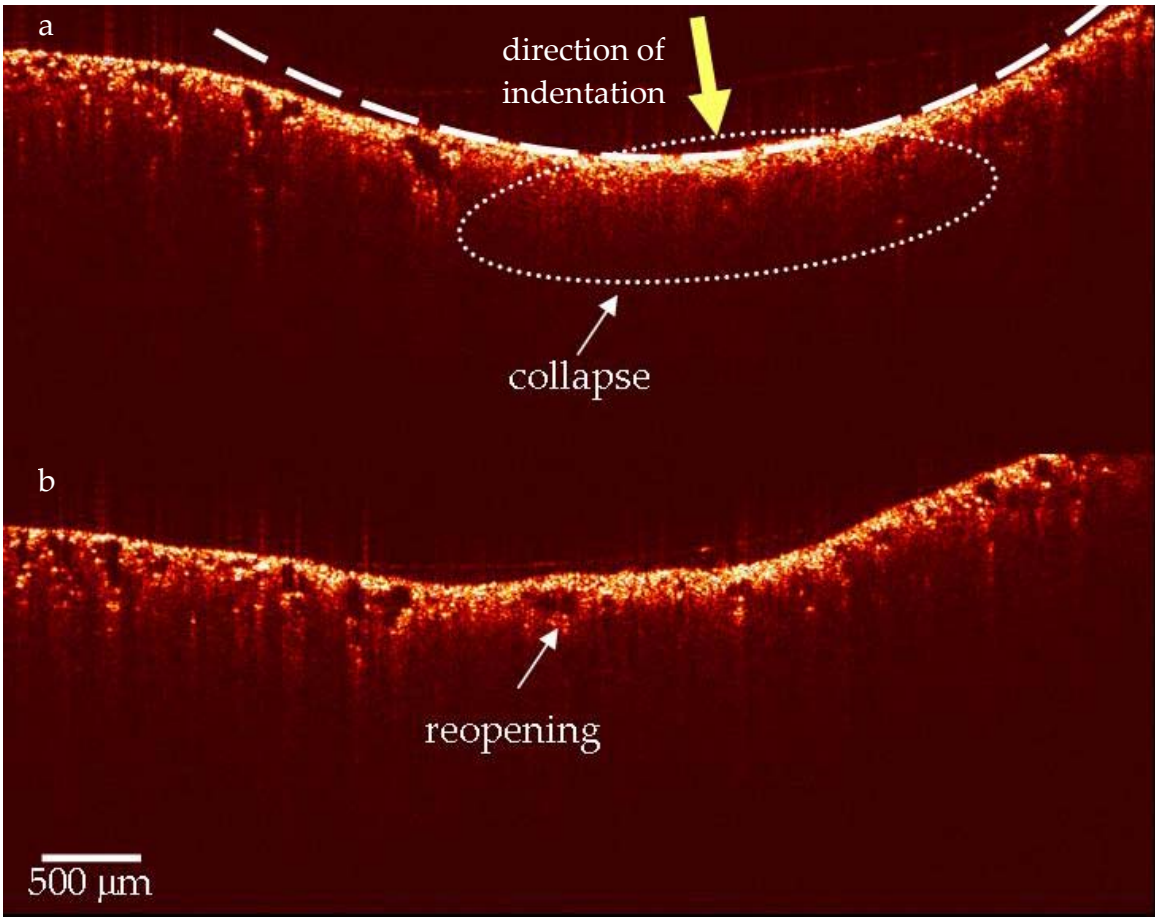

Figure 21. OCT images of a spherically-indented rat lung inflated with air. Image (a) is an imprint left with a 3g load at 10 cmH_2O and (b) is the imprint re-inflated to 18 cmH_2O.

For spherical indentation of rat lungs inflated with blood gas, collapse occurs at the edge of contact as shown in Figure 22. Again, notice that the size of alveoli opened around the region of indentation are much larger than the size of alveoli opened further from the site of indentation. In this image, the larger alveoli are about 300 μm in diameter, while the smaller alveoli appear to be less than 100 μm in diameter.

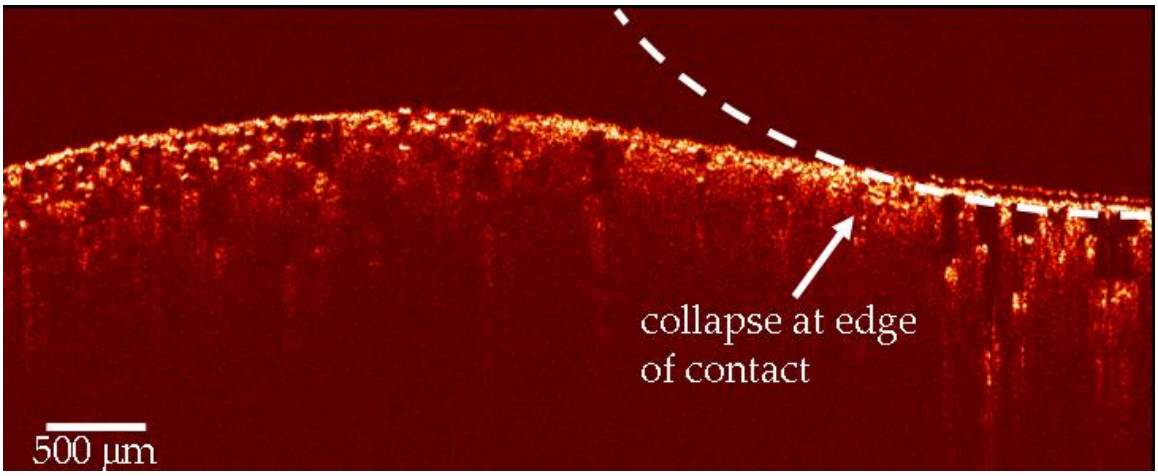

Figure 22. OCT image of a spherically-indented rat lung inflated with blood gas.

Rat lungs were also indented using a cylindrical indenter and Figures 23 and 24 show the results for cylindrical indentation. Figure 23 shows OCT images of indented rat lungs inflated with air. Figure 23a shows collapse underneath the indenter tip, which is evidenced by re-opening of alveoli, shown in Figure 23b, when the lungs were re-inflated to 14 cmH_2O. Figure 23 shows an OCT image of indented rat lungs inflated with blood gas and, once again, collapse is seen underneath the indenter tip.

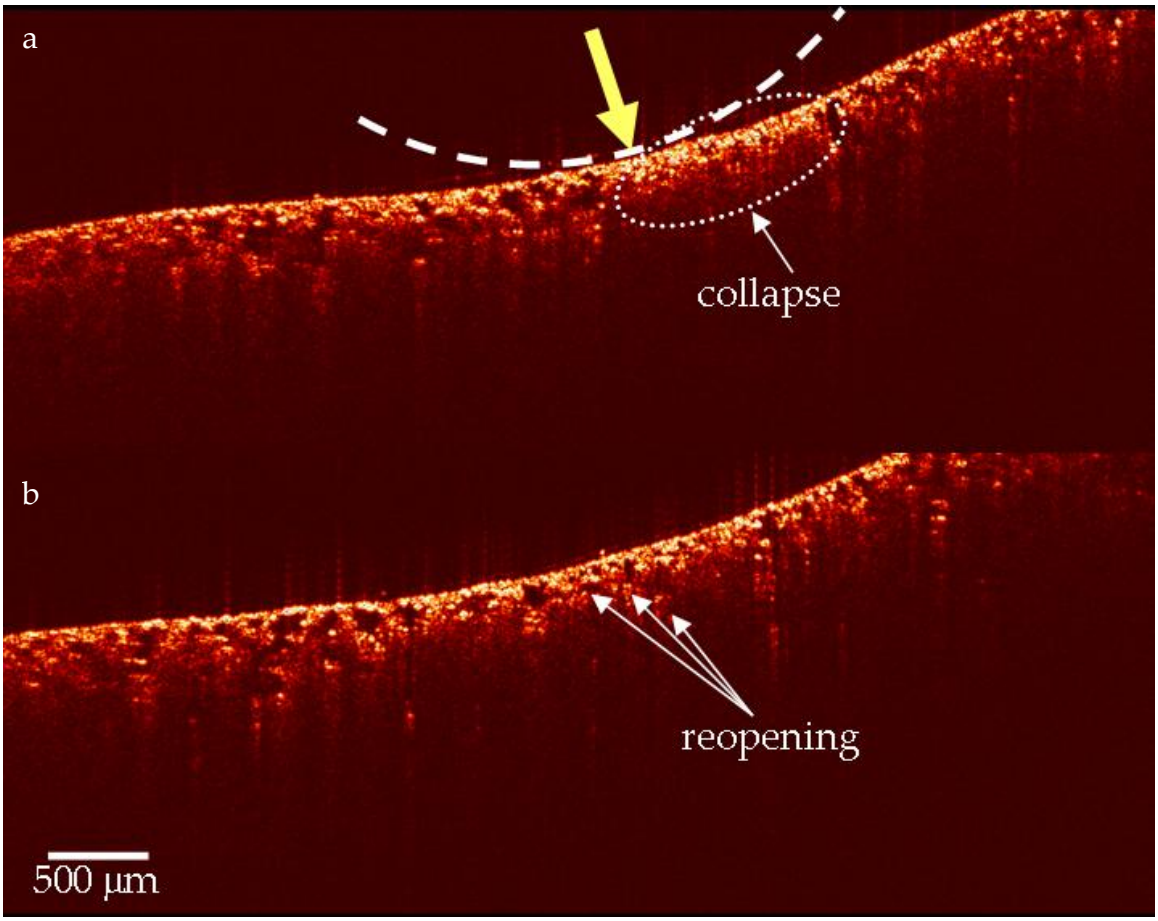

Figure 23. OCT images of a cylindrically-indented rat lung inflated with air. Image (a) is an imprint left at approximately 6 cmH_2O and (b) is the imprint re-inflated to 14 cmH_2O.

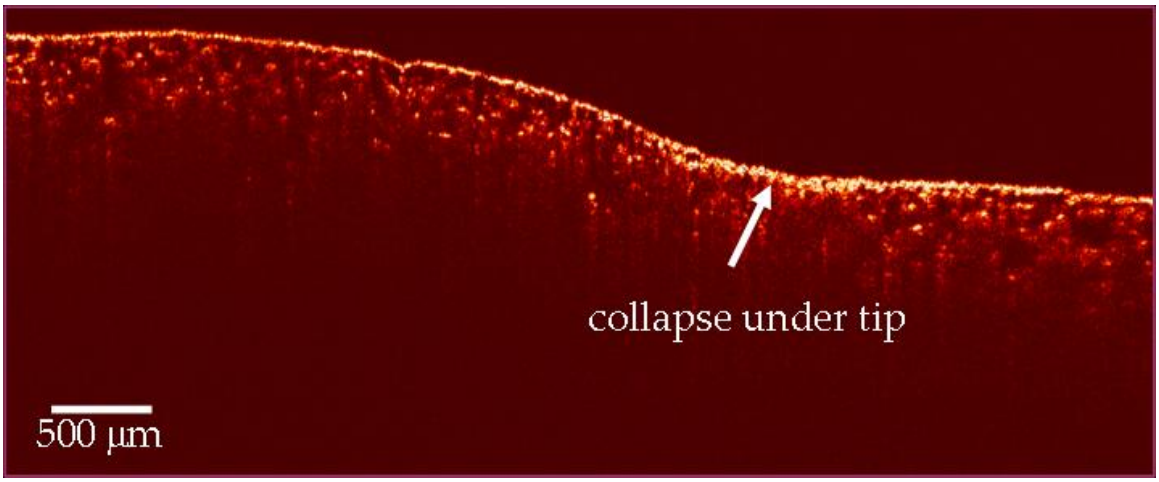

Figure 24. OCT image of a cylindrically-indented rat lung inflated with blood gas.

IX. DISCUSSION

In this study, the effects of inflation pressure and inflation gases on mammalian lungs were examined via spherical indentation. Surface and subsurface plastic deformations were observed, but no numerical criterion was established for the onset of plasticity due to the limitations of the current displacement-controlled indentation set-up as well as the OCT system. For the indenter set-up, load and displacement measurements were easier to obtain during indentation than during unloading. During loading, the piezo buzzers alarmed as soon as measured depths were reached with all the buzzers alarming at the highest marked indentation depth. This allowed easy measurement of the loads at detected depths. However, measuring during unloading was more complicated in that the buzzers were alarming all at once and, therefore, could not be used to indicate specific depths and consequently measured loads. Because the saline solution often kept the silver paint markings connected, the circuit remained closed even after complete unloading was achieved and so the only way to measure depth was to look at when the silver markings no longer touched the lung tissue. Because load and displacement are required measurements during loading and unloading, values of the modulus and the onset of yielding could not be determined. In this study, loading measurements were obtained, but a better indentation set-up will be necessary to obtain accurate measurements during both loading and unloading. For the limitation of the current OCT set-up, *in situ* deformation of the lungs was not observed as the indenter blocked the light source needed to reach the lung tissue in order to

formulate cross-sectional images of the lungs. Therefore, images were taken only before and after indentation, which limits the observation of the onset of plastic deformation and the exact mechanism of alveolar collapse.

Another limitation of the current study is that of time. All of the experiments were limited to one hour, except those with OCT which took more time to set up, to avoid any changes in lung function. According to a study published by van Raemdonck, et al, the warm ischemic tolerance, i.e. the amount of time allowed by the lung without proper blood flow and oxygenation, is limited to only hour, after which time reperfusion injury can occur[39]. This injury occurs at the onset of reperfusion and includes changes such as acute hypoxia, increased peak airway pressure that is known to change the lung compliance, and significant edema formation. In this published study, it was reported that injury was observed with reperfusion 2 hours after warm ischemia, which became worse after 4 hours. No significant changes were seen after 1 hour of warm ischemia, so there is technically a warm ischemic working period of the lungs between 1-2 hours before lung function can be affected. To minimize the changes, the experiments were limited to one hour, but less than 2 hours will not produce significant changes to lung function, which is the time it took to complete the OCT experiments.

In observing the effects of inflation pressure on plastic deformation of the lungs, it was found that the lungs were more dentable at lower pressures than at higher pressures, and that plasticity is observed faster for the lungs inflated at lower pressures. Looking at the graph in Figure 13, a higher load is required to reach even the smallest strain at the higher pressure, 10 cmH_2O. This suggests that inflation with higher pressures make the lungs stiffer, which agrees well with the previous study done by Hajji, Wilson and Lai-Fook that the shear modulus increases with transpulmonary pressure[26]. This is the result of the

effect of the pleural membrane, which according to same study, influences the "displacements caused by forces that are concentrated within a distance which is small compared to T/μ", i.e., the ratio of the pleural membrane tension and the shear modulus[26].

Inflation with the gases used in these experiments is relevant because of the common usage of anesthetics before and during surgery, and of oxygen as a first-line of treatment for patients experiencing acute hypoxia in such cases like asthma. For the effects of these gases on the plastic behavior of lungs, it was found that oxygen made the lungs more dentable whereas isoflurane made the lungs less dentable. For the displacement-controlled indentation, it was also found that isoflurane- and oxygen-inflated lungs shared the same low strain stiffness, but different yield strains. These results were surprising, not because of the differences observed, but how quickly they were observed. During the load- and displacement-controlled experiments, the lungs were exposed to each inflation gas for no longer than 30 minutes. In addition, indentation was done before 30 minutes, and so most of the changes were observed in as little as 5-15 minutes of exposure to one of the three inflation gases. This period of time is a lot shorter than the reported changes in the lungs exposed to isoflurane and oxygen. In a study by Sun, et al., administration of 1.5% isoflurane to patients undergoing surgery increased the alveolar permeability after 1 hour[40]. In a review published by James Crapo, he reported that changes in lung structure due to high oxygen exposure are typically detected after one day or less and cell death follows within 3 days[41]. These changes include changes in cell structures for both type I and type II epithelial cells, which in turn affect the structure of the surfactant. So, published effects of isoflurane and oxygen on the lungs report changes after an hour to a few days. These times are a lot longer than the 5-15 minutes of observed changes in this current study and this may be due to the absence of

perfusion, or blood flow during the experiments, which can serve to remove gas from the air spaces. Without perfusion, the alveolar air spaces are saturated with the introduced gases, and so the pulmonary cells are left to take the load of increased oxygen or isoflurane, thus speeding up the changes typically observed an hour or a day after gas exposure.

Now commenting on the changes observed due to isoflurane exposure, the effects on the dentability as well as the change seen from displacement-controlled indentation may be due to the known bronchodilating effect of the isoflurane. Isoflurane tends to reduce airway resistance[42], i.e. open up the airways, which then allows the alveoli to remain open. This reduces atelectatic tendencies and hence makes the lungs less dentable during indentation. No reports have been found on the effects of isoflurane on the chemistry of the surfactant, but the observed changes may be due to changes in the surfactant as well.

In oxygen-inflated lungs, the degree of dentability and the changes observed from the displacement-controlled indentation may be due to the mentioned saturation of oxygen in the air spaces. With high oxygen exposure, oxygen toxicity can occur even in perfused lungs. In a published report by Burger and Mead, patients exposed to 100% oxygen for 3 hours exhibited difficulty breathing, increased coughing and chest pain[43]. They attributed the changes observed, including changes in the pressure-volume curves compared to lungs exposed to air, to the atelectatic tendencies induced by high oxygen exposure. With this, the increased dentability in unperfused lungs may be the result of oxygen toxicity. However, little is known whether the cellular components are affected first or the surfactant layer that line these cells and so more work will be needed to investigate this further.

To analyze the results of the OCT images, finite element models of the lungs during spherical and cylindrical indentations were made by colleagues who recently submitted the analytical solution to the Journal of Materials Research[44]. Here they used the ABAQUS program to model a lung composed of an elastic solid bound to a top layer that is a pre-tensed, elastic membrane with no bending resistance. The modulus was modeled as comparable to those measured in the breathing inflation range presented by Hajji, Wilson and Lai-Fook[26], and the tension was observed to be nearly constant during indentation. The nonlinear geometry (NLGEOM) option was also included to allow for large deformations. Several stress distributions including that of pressure and Mises stresses were modeled and it was found that the experimental results agrees with the pressure distribution model.

Figures 25 and 26 show the pressure distribution models for axisymmetric (spherical), and rib (cylindrical) indentation, respectively. From these models, good agreement between the regions of high compressive pressure and regions of lung collapse were observed. In the case of the axisymmetric model, the highest compressive pressure initiates underneath the indenter tip, but shifts toward the edge of contact with deeper indentation. This same behavior is seen in Figures 21 and 22, where in Figure 22 the lungs were exposed to 5% isoflurane for a much longer period than when they were inflated with blood gas. Therefore, considering the effects of the isoflurane instead of the high concentration of oxygen, the lungs shown in Figure 22 are less dentable and so require higher strains to produce a similar dent, which is why collapse at the edge of contact is observed. In the case of the rib model, the highest compressive pressure remains underneath the indenter tip. Again this model agrees well with the experimental results as seen in the OCT images in Figures 23 and 24.

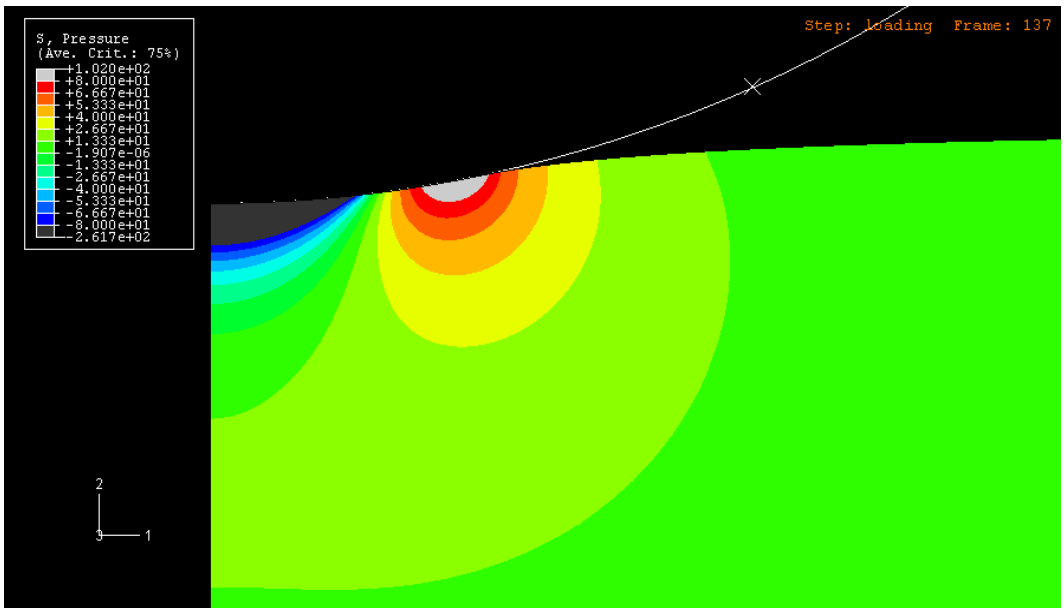

Figure 25. Pressure distribution for axisymmetric indentation of an elastic half-space bound by a pre-tensed elastic membrane.

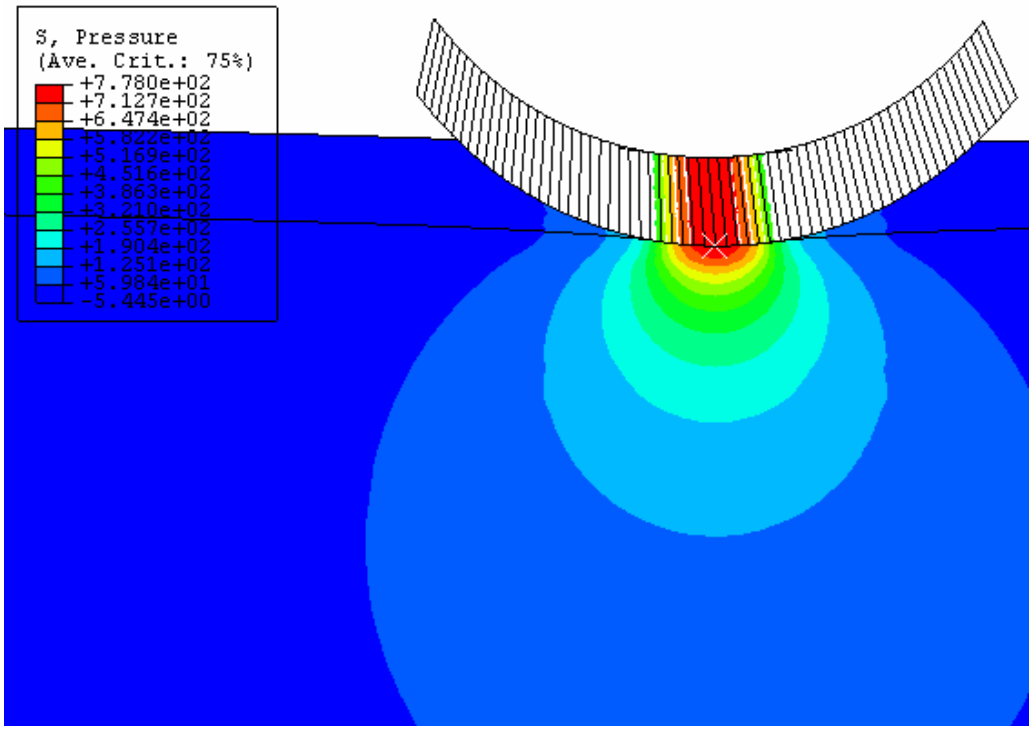

Figure 26. Pressure distribution for "rib" indentation of an elastic half-space bound by a pre-tensed elastic membrane.

X. CONCLUSION AND FUTURE WORK

With spherical indentation, the roles of inflation pressure and inflation gases were tested. The lungs are stiffer when inflated at a higher pressure and are most dentable when inflated with oxygen, then with air, and last with isoflurane. With the three inflation gases, the lungs also share the same low strain stiffness, but with different yield strains. With optical coherence tomography, sub-surface plastic deformation was observed. In comparing the OCT images from the experiments to the FE models for both spherical and cylindrical indentation, a compressive pressure criterion for alveolar collapse is established.

Due to the limitations of the current indenter set-up, more work will be needed to accurately calculate the modulus and determine the onset of yielding with spherical indentation. A plan to build an automated bio-indenter is already established which will incorporate a force transducer to measure the load and a stepper motor to allow for precise measurements of displacement. Due to the limitations of the OCT system, more planning will be done to find a solution that will allow *in situ* imaging of deformation during indentation, which may or may not include the use of a transparent spherical or hemispherical glass or plastic as an attachment to the indenter system that will allow the laser of the OCT system to pass. Lastly, considering the lack of studies comparing the effects of inflation gases on the microstructure of the lungs and the surfactant, the next step will be to look closer at both the microstructure of the lungs and the chemistry of the

surfactant simultaneously to determine which gets affected first to cause the changes that have been observed thus far.

In conclusion, even with the limitations mentioned, in studying the effects of various inflation pressures and inflation gases, spherical indentation and optical coherence tomography proved successful in studying non-uniform plastic deformation of the lungs that are relevant to both healthy and pathological conditions.

REFERENCES

1. West, J.B., *Respiratory Physiology - The Essentials*. 1974, Baltimore: Waverly Press. 185.
2. Creuwels, L.A.J.M., L.M.G.v. Golde, and H.P. Haagsman, *The pulmonary surfactant system: biochemical and clinical aspects.* Lung, 1997. **175**: p. 1-39.
3. Mercer, R.R., M.L. Russell, and J.D. Crapo, *Alveolar septal structure in different species.* Journal of Applied Physiology, 1994. **77**(3): p. 1060-1066.
4. Udobi, K.F., E. Childs, and K. Touiijer, *Acute respiratory distress syndrome.* American Family Physician, 2003. **67**(2): p. 315-322.
5. Mortelliti, M.P. and H.L. Manning, *Acute respiratory distress syndrome.* American Family Physician, 2002. **65**(9): p. 1823-1830.
6. Demoule, A., et al., *Relationship between pressure-volume curve and markers for collagen turn-over in early acute respiratory distress syndrome.* Intensive Care Medicine, 2006. **32**: p. 413-420.
7. Barnes, P.J., *Small airways in COPD.* New England Journal of Medicine, 2004. **350**(26): p. 2635-2637.
8. Klassen, T., W.M. Thurlebeck, and N. Berend, *Correlation between lung structure and function in a canine model of emphysema.* Journal of Applied Physiology, 1981. **51**(2): p. 321-326.
9. Sutherland, E.R. and R.M. Cherniack, *Management of chronic obstructive pulmonary disease.* New England Journal of Medicine, 2004. **350**: p. 2689-2697.
10. Sarnaik, A.P., et al., *Pressure-controlled ventilation in children with severe status asthmaticus.* Pediatric Critical Care Medicine, 2004. **5**(2): p. 133-138.
11. Hoppin, F.G., Jr., *Parenchymal mechanics and asthma.* Chest, 1995. **107**(3): p. 140S-144S.
12. Gajic, O., et al., *Ventilator settings as a risk factor for acute respiratory distress syndrome in mechanically ventilated patients.* Intensive Care Medicine, 2005. **31**: p. 922-926.
13. Whitehead, T. and A.S. Slutsky, *The pulmonary physician in critical care * 7: Ventilator induced lung injury.* Thorax, 2002. **57**(7): p. 635-642.
14. Dreyfuss, D. and G. Saumon, *Ventilator-induced lung injury: lessons from experimental studies.* American Journal of Respiratory and Critical Care Medicine, 1998. **157**: p. 294-323.

15. Gattinoni, L., et al., *Physical and biological triggers of ventilator-induced lung injury and its prevention.* European Respiratory Journal, 2003. **22**(Supplement 47): p. 15s-25s.
16. Vlahakis, N.E. and R.D. Hubmayer, *Cellular stress failure in ventilator-injured lungs.* American Journal of Respiratory and Critical Care Medicine, 2005. **171**: p. 1328-1342.
17. *Lung Biology in Health and Disease: Bioengineering Aspects of the Lung.*, ed. J.B. West. Vol. 3. 1977, New York: Marcel Dekker. 583.
18. Suki, B., et al., *Biomechanics of the lung parenchyma: critical roles of collagen and mechanical forces.* Journal of Applied Physiology, 2005. **98**: p. 1892-1899.
19. Oldmixon, E.H. and F.G. Hoppin, Jr., *Comparison of amounts of collagen and elastin in pleura and parenchyma of dog lung.* Journal of Applied Physiology, 1984. **56**(5): p. 1383-1388.
20. Mead, J., T. Takashima, and D. Leith, *Stress distribution in lungs: a model of pulmonary elasticity.* Journal of Applied Physiology, 1970. **28**(5): p. 596-608.
21. Hajji, M.A., *Indentation of a membrane on an elastic half space.* Journal of Applied Mechanics, 1978. **45**: p. 320-323.
22. Hajji, M.A., *Indentation of a membrane on an elastic half space with application to material testing of inflated lung lobes.*, in *Department of Aerospace Engineering and Mechanics*. 1978, University of Minnesota: Minneapolis. p. 108.
23. Coughlin, M.F., B. Suki, and D. Stamenovic, *Dynamic behavior of lung parenchyma in shear.* Journal of Applied Physiology, 1996. **80**(6): p. 1880-1890.
24. Duggan, M. and B.P. Kavanagh, *Pulmonary atelectasis: a pathogenic perioperative entity.* Anesthesiology, 2005. **102**(4): p. 838-854.
25. Lai-Fook, S.J. and R.E. Hyatt, *Effects of age on elastic moduli of human lungs.* Journal of Applied Physiology, 2000. **89**: p. 163-168.
26. Hajji, M.A. and T.A. Wilson, *Improved measurements of shear modulus and pleural membrane tension of the lung.* Journal of Applied Physiology, 1979. **47**(1): p. 175-181.
27. Oliver, W.C. and G.M. Pharr, *Measurement of hardness and elastic modulus by instrumented indentation: Advances in understanding and refinements to methodology.* Journal of Materials Research, 2004. **19**(1): p. 3-20.
28. Fujisawa, N., W. Li, and M.V. Swain, *Observation and numerical simulation of an elastic-plastic solid loaded by a spherical indenter.* Journal of Materials Research, 2004. **19**(12): p. 3474-3483.
29. Tabor, D., *The Hardness of Metals*. 1951, Oxford: Clarendon Press. 175.
30. Alper, J., *OCT: Images of coherence.* Science, 1993. **261**(5121): p. 555.

31. Brezinski, M.E., *Optical coherence tomography: principles and applications.* 2006, Burlington: Academic Press.
32. Han, C.W., et al., *Analysis of rabbit articular cartilage repair after chondrocyte implantation using optical coherence tomography.* Osteoarthritis and Cartilage, 2003. **11**: p. 111-121.
33. Hanna, N., et al., *Two-dimensional and 3-dimensional optical coherence tomographic imaging of the airway, lung, and pleura.* Journal of Thoracic and Cardiovascular Surgery, 2005. **129**(3): p. 1287-1293.
34. Huang, D., *Optical coherence tomography.* Science, 1991. **254**(5035): p. 1178-1181.
35. Singer, A., et al., *Optical coherence tomography: a noninvasive method to assess wound reepithelialization.* Acad Emer Med, 2007. **14**(5): p. 387-391.
36. Sutedja, G., *New techniques for early detection of lung cancer.* European Respiratory Journal, 2003. **21**(Suppl. 39): p. 57s-66s.
37. Whiteman, S.C., et al., *Optical coherence tomography: real-time imaging of bronchial airways microstructure and detection of inflammatory/neoplastic morphologic changes.* Clinical Cancer Research, 2006. **12**(3): p. 813-818.
38. Andersen, P., *Introduction: Optical Coherence Tomography.* 2004, Optics and Plasma Research Department, Riso National Laboratory: Denmark.
39. Van Raemdonck, D.E.M., et al., *Warm ischemic tolerance in collapsed pulmonary grafts is limited to 1 hour.* Annals of Surgery, 1998. **228**(6): p. 788-796.
40. Sun, S.S., et al., *Transient increase in alveolar epithelial permeability induced by volatile anesthesia with isoflurane.* Lung, 2000. **178**: p. 129-135.
41. Crapo, J.D., *Morphologic changes in pulmonary oxygen toxicity.* Annual Review of Physiology, 1986. **48**: p. 721-731.
42. Ruiz, P. and D. Chartrand, *The effect of isoflurane 0.6% on respiratory mechanics in anesthetized-paralyzed humans is not increased at concentrations of 0.9% and 1.2%.* Canadian Journal of Anesthesia, 2003. **50**(1): p. 67-70.
43. Burger, E.J. and J. Mead, *Static properties of lungs after oxygen exposure.* Journal of Applied Physiology, 1969. **27**(2): p. 191-197.
44. Kim, J.H. and A. Gouldstone, *Analytical solution for indentation of an elastic half-space bound by a pre-tensed elastic membrane.* 2007, Stony Brook University.